Drug Design, Development and Therapy Dovepress

Open Access Full Text Article ORIGINAL RESEARCH

16S rRNA Gene Sequencing Combined with Metabolomics to Explore Intestinal Flora and Metabolic Changes in Young Febrile Rats and the Mechanism of Xiangqin Jiere Granules

Xiying He[1,2], Min Pan[2], Xinchen Wu[1], Huayan Li[1], Yujiang Xi[1], Lijuan Zhang[3], Yi Zhang[2], Yakai Tian[4], Ruirui Wang[2], Lei Xiong[1]

[1]The First School of Clinical Medicine, Yunnan University of Chinese Medicine, Kunming, People's Republic of China; [2]College of Chinese Materia Medica, Yunnan University of Chinese Medicine, Kunming, People's Republic of China; [3]School of Basic Medical Sciences, Yunnan University of Chinese Medicine, Kunming, People's Republic of China; [4]College of Animal Science and Technology, Yunnan Agricultural University, Kunming, People's Republic of China

Correspondence: Lei Xiong; Ruirui Wang, Yunnan University of Chinese Medicine, 1076 Yuhua Road, Kunming, 650500, People's Republic of China, Tel +86 13987676677, Email xlluck@sina.com; wangrryucm@126.com

Purpose: Xiangqin Jiere Granules (XQJRG), a Chinese patent medicine used to treat acute fever in children caused by colds, seasonal flu, and coronavirus disease 2019 has been proven to have antipyretic and anti-inflammatory effects in young febrile rats. Fever is known to affect the host-gut microbiota crosstalk. However, the pharmacological mechanism of XQJRG in this regard remains unclear.

Methods: This study utilized a young febrile rat model previously reported by our team and extended the rat body temperature monitoring period following drug administration to explore the differences in efficacy between XQJRG and the commonly used pediatric antipyretic ibuprofen. Subsequently, the colonic contents of rats were analyzed using 16S rRNA gene sequencing and untargeted metabolomics. The short-chain fatty acid content was quantified using high-throughput targeted metabolomics. The expression of short-chain fatty acid receptors and pro-inflammatory genes in the colonic tissue was evaluated using quantitative real-time PCR, Western blot, and enzyme-linked immunosorbent assay.

Results: XQJRG showed a longer antipyretic duration than ibuprofen. XQJRG improved dysbiosis of the intestinal microbiota in young febrile rats, bringing its flora composition closer to that of normal rats. It significantly increased the relative abundance of *s_Phascolarctobacterium_faecium* and *s_Roseburia_sp*. related to the production of short-chain fatty acids (SCFAs), the contents of butyric acid and nonanoic acid and protein levels of SCFAs receptor GPR41. Moreover, XQJRG significantly increased the levels of metabolites with anti-inflammatory effects, reduced the contents of metabolites directly associated with fever, and decreased the levels of pro-inflammatory cytokines interleukin-1β and monocyte chemotactic protein-1 in the colon of young febrile rats to normal levels.

Conclusion: XQJRG exhibited a more stable and persistent antipyretic effect in young febrile rats compared to ibuprofen. Its mechanism was at least partially attributed to regulating intestinal flora disorders, increasing anti-inflammatory metabolites, and inhibiting the production of inflammatory factors in young febrile rats.

Keywords: Pediatric fever, gut microbiota, metabolomics, antipyretic, anti-inflammatory, Xiangqin Jiere Granules

Introduction

Fever is a main symptom of common childhood illnesses, including the common cold, seasonal influenza, and coronavirus disease 2019 (COVID-19), and studies have shown that the intestinal flora of febrile children is imbalanced.[1] It is well known that acute fever in children is usually caused by infection, and the gut, as the largest immune organ, has a resident microbiota that is believed to shape children's immune systems.[2] Gut flora can help the host resist the invasion of foreign bacteria and the expansion of opportunistic pathogens. For example, *Lactobacillus* and *Bifidobacterium* have been shown to have definitive antiviral activity against respiratory viruses, especially the influenza

Received: 19 May 2024
Accepted: 19 November 2024
Published: 27 November 2024

Graphical Abstract

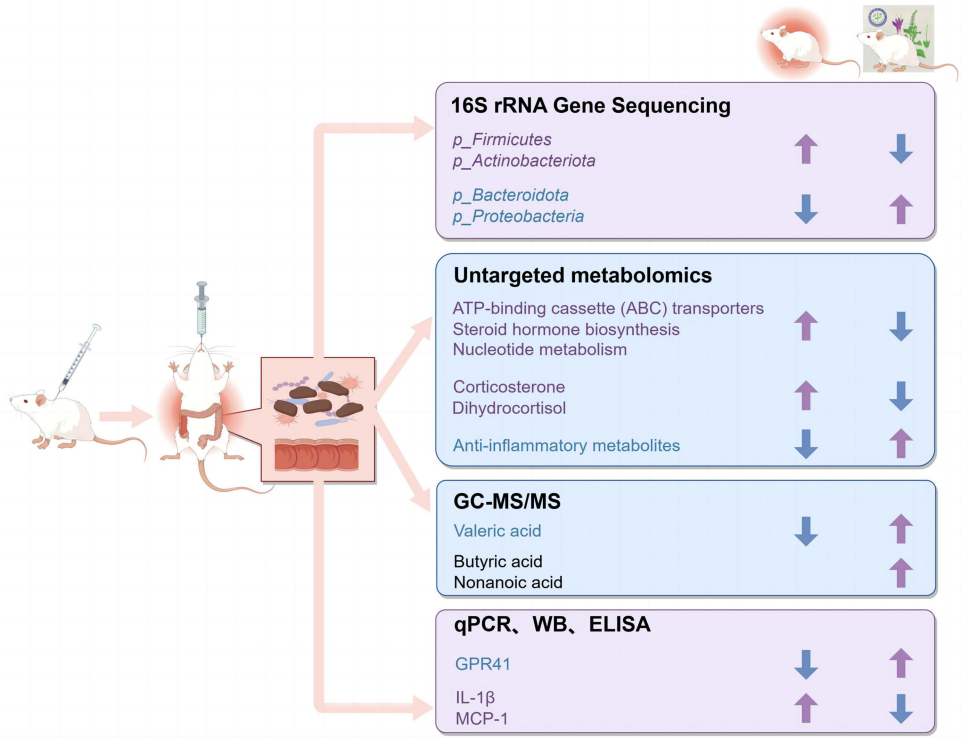

A virus.[3] Meanwhile, intestinal flora produces metabolites, including short-chain fatty acid (SCFA) and bile acid, which participate in host immune regulation. Recent studies confirmed that gut flora was a key regulator of body temperature changes in health and critical illness, and the febrile responses in humans and mice with pathogenic infections were influenced by gut bacteria.[4] Considering the many gastrointestinal side effects of antipyretics currently available for children, attention has begun to turn to natural and traditional Chinese medicine (TCM) with antipyretic properties. At present, single Chinese medicines such as Bupleuri Radix, Scutellariae Radix, Coptis chinensis, Rheum palmatum, Chuanxiong Rhizome, Cinnamomi Ramulus, Indigo Naturalis, Forsythiae Fructus, Lonicera Japonica Flos, Ephedrae Herba, Gypsum Fibrosum, Gardeniae Fructus, Bubali Cornu, Houttuyniae Herba, Andrographis Herba, and Puerariae Lobatae Radix, as well as Chinese patent medicines such as Qingkailing Injection, Shuang-Huang-Lian Preparation, Jinxin oral liquid, Yin Qiao San, Hao Jia Xu Re Qing Granules and Reduning injection, have been proven to have significant antipyretic effects.[5–8]

Xiangqin Jiere Granules (XQJRG) is an effective proprietary Chinese medicine that has been used clinically for nearly 10 years to treat febrile illnesses in children, and its therapeutic efficacy has been confirmed in clinical studies and animal experiments.[9–14] The formula is composed of Pogostemon cablin (*Pogostemon cablin* Benth)., Scutellaria baicalensis (*Scutellaria baicalensis* Georgi), Radix bupleuri (*Bupleurum chinense* DC)., Artemisia annua (*Artemisia annua* L)., Forsythia suspensa (*Forsythia europaea* Degen & Bald)., Isatidis folium (*Isatis tinctoria* L) and Gypsum fibrosum. Our previous study showed that it reduces plasma levels of pro-inflammatory factors interleukin (IL)-1β, IL-6, tumor necrosis factor (TNF)-α, and hypothalamic inflammatory mediator cyclooxygenase (COX)-2 and prostaglandin E2 (PGE2) in young febrile rats.[9] However, whether these antipyretic and anti-inflammatory effects are related to the regulation of the host intestinal flora and metabolism remain unclear.

In fact, as a complex mixture of natural compounds, only a portion of the active ingredients of TCM can be directly absorbed into the circulation orally, while the other portion is metabolized by the intestinal flora into new active

compounds, which in turn exert biological effects.[15] For example, studies on *Scutellaria baicalensis*, one of the herbs in XQJRG, have confirmed that its main constituent, baicalin, is difficult to absorb through the gastrointestinal tract in its natural form and exhibits stronger anti-inflammatory effects after being metabolized by gut microorganisms into baicalein and oroxylin A.[16] Based on abundant evidence that the efficacy of TCM is largely attributed to modulation by intestinal flora and host metabolism, the research approach of integrating intestinal flora with metabolomics has seen growing application in elucidating the mechanisms of action behind TCM,[17–19] including antipyretic mechanisms.[20,21]

This study aimed to investigate whether XQJRG could alleviate yeast-induced fever and inflammation by modulating gut flora and host metabolism. First, 16S rRNA sequencing was used to explore changes in the intestinal flora of young febrile rats, and an untargeted metabolomics approach was used to investigate changes in the metabolic profiles of the intestinal contents. Subsequently, high-throughput targeted metabolomics was used to detect SCFA content. Finally, quantitative real-time PCR (qPCR), Western blot (WB), and enzyme-linked immunosorbent assay (ELISA) were used to detect the levels of G-protein coupled receptor (GPR) 41, GPR43, and GPR109A, the receptor for SCFAs, as well as pro-inflammatory genes IL-1β, IL-6, IL-18, and MCP-1 in colon tissues. Thus, the association between the antipyretic and anti-inflammatory effects of XQJRG and the intestinal flora and metabolites in young febrile rats was explored.

Materials and Methods

*2.1 Medicine and Reagents*XQJRG was purchased from the Yunnan Provincial Hospital of Traditional Chinese Medicine (batch number: 20230329, China). Yeast was purchased from Angle Yeast Co. Ltd. (batch number: CY20230509, Yichang, China). Ibuprofen was purchased from Shanghai Johnson Pharmaceutical Co. Ltd. (batch number: 211016419; Shanghai, China). Physiological saline was purchased from Kunming Nanjiang Pharmaceutical Co., Ltd. (batch number: C22083001; Kunming, China).

Animals and Treatments

The study was approved by the Ethics Committee of Yunnan University of Chinese Medicine (ethical code no. R-062022014), and we comply with the provisions of national standard "Laboratory animal—Guideline for ethical review of animal welfare (GB/T 35892–2018)" to ensure the welfare of the experimental animals used in our research. The experimental protocol is consistent with that described in our previous study.[9] Specifically, twenty-four Sprague–Dawley (SD) rats aged 4–6 weeks and weighing 120–150 g were adaptively fed for 3 days and then randomly divided into four groups of six rats: the control group (CG), model group (MG), ibuprofen group (BG), and XQJRG group (XG). On the day of the experiment, after measuring the basal body temperature of all rats, rats in the MG, BG, and XG were subcutaneously administered a yeast suspension (10 mg/kg) in the back of the neck, and rats in the CG were administered physiological saline at the same location. When the body temperature of the rats receiving the yeast injection increased by more than 0.8 °C at the sixth hour, the CG and MG rats were given ultrapure water orally, and the BG and XG rats received ibuprofen (5.73 mg/100 g) and XQJRG (0.29 g/100 g) by intragastric administration, respectively. The rats were monitored for changes in body temperature and sacrificed after the final temperature measurement. Because the antipyretic mechanism of ibuprofen is the inhibition of COX activity, which reduces the production of the febrile mediator PGE2, with little contribution of intestinal flora to its efficacy, only the colon contents of CG, MG, and XG rats were collected and immediately placed into liquid nitrogen, and subsequent microbiomics, metabolomics, and SCFA assays were performed by Biotree Tech (Shanghai, China). Notably, one sample from the XG (XG2) was excluded from the multi-omics analysis because it had a much lower amplicon sequence variant (ASV) number than all the other samples in microbial 16s rRNA sequencing and did not cluster with the other samples of the same group in both principle components analysis (PCA) and orthogonal projections to latent structures discriminant analysis (OPLS-DA) of metabolomics. Colon tissues were collected from all rats for subsequent molecular biology study.

2.3 16S rRNA Gene Sequencing

The total DNA of the microbiome was extracted using the cetyltrimethylammonium bromide method, DNA extraction quality was detected by agarose gel electrophoresis, and DNA was quantified using a UV spectrophotometer. The V3-V4 region was PCR amplified using primers (341F: 5'-CCTACGGGNGGCWGCAG-3' and 805R: 5'-

GACTACHVGGGTATCTAATCC-3'). After purification using AMPure XT beads (Beckman Coulter Genomics, Danvers, MA, USA) and quantification by Qubit (Invitrogen, USA), PCR products were evaluated using an Agilent 2100 Bioanalyzer (Agilent, USA) and Illumina (KapaBiosciences, Woburn, MA, USA) library quantification kits. The concentration of the qualified library exceeded 2nM. Qualified sequencing libraries (index sequences were not reproducible) were gradient-diluted, mixed in the appropriate ratio according to the desired sequencing volume, denatured to single-stranded DNA using sodium hydroxide and sequenced using the NovaSeq 6000 SP Reagent Kit (500 cycles) on a NovaSeq 6000 sequencer for 2×250 bp double-end sequencing. The data obtained were processed by the divisive amplicon denoising algorithm (DADA2) to obtain the ASV feature sequences. The raw sequence counts for each sample were rarefied to a uniform sequencing depth of 69,573 sequences per sample using the R package vegan. Then diversity analysis, flora classification annotation, and difference analysis were carried out.

Untargeted Metabolomics Study

The intestinal contents were weighed 25 mg and 500 uL of extraction solution (methanol: acetonitrile: water = 2:2:1 (V/V) containing isotope-labeled internal standard) was added. The mixture was milled in a grinder at 35 hz for 4 min and sonicated for 5 min in an ice-water bath; this operation was repeated three times. After resting at −40 °C for 1 h, the mixtures were centrifuged at 12,000 rpm for 15 min at 4 °C, and the supernatants were transferred to injection bottles for detection. Equal amounts of supernatant from all samples were collected and mixed as quality control samples for detection. Chromatographic separation of the target compounds was performed on the Waters ACQUITY UPLC BEH Amide (2.1 mm × 50 mm, 1.7 μm) liquid chromatography column using the Vanquish (Thermo Fisher Scientific) ultra-high performance liquid chromatograph. The liquid chromatographic phase A was an aqueous phase containing 25 mm ammonium acetate and 25 mmol/L ammonia, whereas phase B was acetonitrile. The temperature of the sample plate was 4 °C, and the injection volume was 2 μL. Primary and secondary mass spectrometry data were collected using the Orbitrap Exploris 120 mass spectrometer with Xcalibur software (version 4.4, Thermo). The parameters were set as follows: sheath gas flow rate as 50 Arb, Aux gas flow rate as 15 Arb, capillary temperature 320 °C, full mass spectrometry (MS) resolution as 60000, tandem MS (MS/MS) resolution as 15000, collision energy: SNCE 20/30/40, spray voltage as 3.8 kV (positive) or −3.4 kV (negative), respectively. After the raw data were converted into mzXML format using ProteoWizard software, peak identification, extraction, and alignment were performed using an independently written R program package (kernel XCMS). Subsequently, the peaks were matched to the self-constructed secondary mass spectrometry database BiotreeDB (V2.1) for substance annotation.

Identification and Quantification of SCFAs by Gas Chromatography Tandem Mass Spectrometry Analysis

Approximately 50 mg of intestinal contents was placed into 2 mL Eppendorf (EP) tubes with 1 mL of purified water and vortexed for 10s. Steel beads were added and homogenized with a grinder at 40 hz for 4 min, ultrasonicated for 5 min (incubated in ice water) and repeated three times. The samples were centrifuged at 5000 rpm for 20 min at 4 °C, and 0.8 mL of supernatant was transferred to a new 2 mL EP tube with 0.1 mL of 50% H_2SO_4 and 0.8 mL of internal standard solution (containing internal standards 2-methylpentanoic acid and methyl tert-butyl ether), vortexed for 10s, oscillated for 10 min, and ultrasonicated for 10 min (incubated in ice water). The samples were centrifuged again at 10,000 rpm for 15 min at 4 °C and kept at −20 °C for 30 min. The supernatant was transferred into a fresh 2 mL glass vial. Subsequent gas chromatography tandem mass spectrometry (GC-MS/MS) analysis was performed using a SHIMADZU GC2030-QP2020 NX gas chromatography-mass spectrometer. The system utilized an HP-FFAP capillary column (30 m×250 μm×0.25 μm, J&W Scientific, Folsom, CA, USA). A 1 μL aliquot of the analyte was injected in split mode (5:1). Helium was used as the carrier gas, the front inlet purge flow was 3 mL min^{-1}, and the gas flow rate through the column was 1.2 mL min^{-1}. The initial temperature was kept at 50 °C for 1 min, then raised to 150 °C at a rate of 50 °C min^{-1} for 1 min, to 170 °C at a rate of 10 °C min^{-1}, to 225 °C at a rate of 20 °C min^{-1} for 1 min, to 240 °C at a rate of 40 °C min^{-1} for 1 min. The injection, transfer line, quad, and ion source temperatures were 220 °C, 240 °C, 150 °C and 200 °C, respectively. The energy was −70 eV in electron impact mode. MS data were acquired in the scan/SIM mode

with an m/z range of 33–150 after a solvent delay of 3.75 min. Standard curves of the 11 SCFAs were established by configuring chemical standards with different concentration gradients, from which the absolute SCFA content in each sample was calculated.

Reverse Transcription-Quantitative Polymerase Chain Reaction

Total RNA was extracted using TRIzol reagent (Invitrogen, 15596018), and reverse transcription (RT) was performed using a quantitative PCR reverse transcription reagent (Takara, RR047B). Two-step RT-PCR was performed to amplify the cDNA on the Bio-Rad CFX Connect ™ Real-Time PCR System with TB Green® Premix Ex Taq™ II (TAKARA, RR820A), and the reaction condition was set to 95 °C for 2 min, followed by 39 cycles of 95 °C for 5 s and 60 °C for 30s. The relative expression of the target genes was calculated using the 2-ΔΔCt method with GAPDH as the internal reference gene and using the average Ct value of duplicate samples for each sample. The primer sequences are listed in Table S1.

Western Blot

Total protein was extracted using RIPA Lysis Buffer (Beyotime, P0013B) containing phenylmethylsulfonyl fluoride Solution (Beyotime, ST507-10 mL). The protein concentration of the samples was assessed using the Enhanced BCA Protein Assay Kit (Beyotime, P0010), followed by dilution to ensure a uniform protein concentration across all samples. SDS-PAGE Loading Buffer (Cwbio, CW0027S) was added, and the mixture was boiled at 100 °C for five min to induce protein denaturation. Equal amounts of samples were subjected to 12% sodium dodecyl sulfate polyacrylamide gel electrophoresis (SDS-PAGE) electrophoresis and subsequently transferred onto polyvinylidene difluoride membranes in an ice bath. Following the blocking step, GPR41 (PA5-75521, Thermo Fisher Scientific, 1:1000) secondary antibodies (included in the kit) were added according to the instructions provided in the Novel One-Step Western Blot Kit (rabbit) (Sangon Biotech, C510049). Beta Actin (20536-1-AP, Proteintech, 1:5000) was utilized as a control. After color development using BeyoECL Moon (Extreme hypersensitivity ECL chemiluminescence kit) (Beyotime, P0018FS), protein bands were captured using a chemiluminescence imaging system (Servicebio, SCG-W2000, China), and grayscale intensity analysis was conducted using ImageJ software.

Statistical Analysis

Data were processed using SPSS (Version 23.0. Armonk, NY: IBM Corp)., and expressed as mean ± standard error of the mean (SEM). Comparisons between multiple groups were performed using one-way analysis of variance and plotted using GraphPad Prism 9.0.0 software (www.graphpad.com). The p-value < 0.05 was considered statistically different.

Results

XQJRG Significantly Reduced the Body Temperature of Young Yeast-Induced Febrile Rats

At the onset of the experiment, there were no statistically significant differences in body temperature among the rats ($P>0.05$). After 6 h, except for the CG, an increase in body temperature was observed in all rats ($P<0.001$). From 8–12 h, the body temperature of febrile rats treated with BG and XQJRG was reduced ($P<0.001$), which is consistent with our previous findings. Throughout 12–16 h, the body temperature of rats administered XQJRG continued to decline, approaching that of normal rats. However, rats treated with BG exhibited an increasing trend in body temperature, which gradually approached that of febrile rats in the MG (Figure 1).

XQJRG Restored Intestinal Flora Homeostasis in Young Febrile Rats

Analysis of the Intestinal Flora Diversity

A total of 4425 ASV feature sequences were obtained from the raw data. α-diversity and beta-diversity were employed to investigate the impact of XQJRG on the diversity and dissimilarity of intestinal microbiota in young febrile rats. As shown, the Chao1, Shannon, and Simpson indices of α-diversity showed no statistically significant differences among the three groups (Figure 2A–C). Beta diversity analysis was conducted using principal coordinate analysis based on unweighted UniFrac distance,

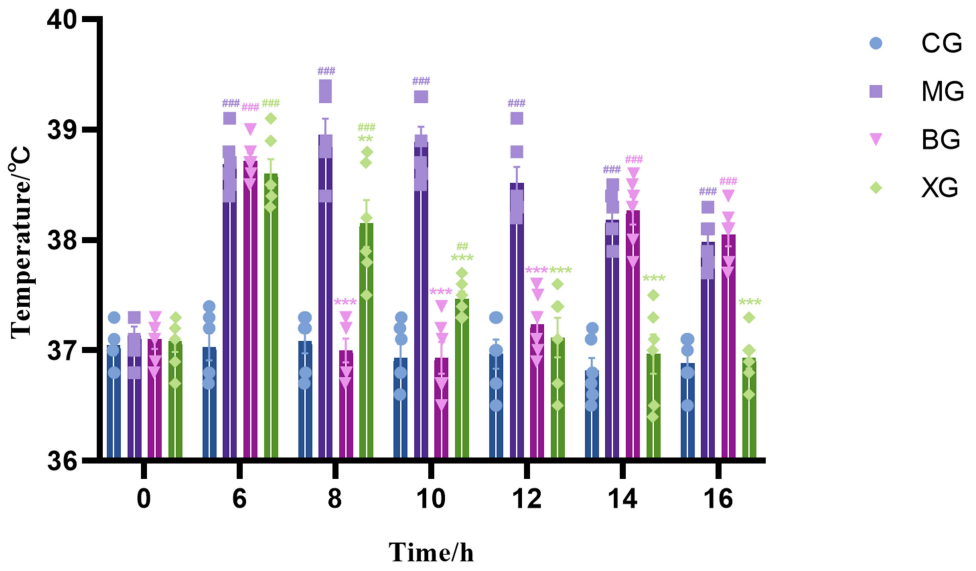

Figure 1 Change in body temperature in young febrile rats. Data are expressed as the mean ± SEM (n = 6). At the same point in time, compared to CG, $^{\#\#}P<0.01$, and $^{\#\#\#\#}P<0.001$; compared to MG, $^{**}P<0.01$, and $^{***}P<0.001$.

which revealed distinct clustering patterns. As illustrated in Figure 2D, the samples from the MG were entirely separate from those of the CG and XG, whereas some samples from the XG were relatively close to those of the CG. These results indicate significant changes in the flora abundance distribution within the intestinal microbiota of young febrile rats, which were effectively reversed by treatment with XQJRG.

Analysis of the Intestinal Flora Composition

Stacked bar charts visually showed the top 30 phylum and genus in relative abundance in each of the three groups (Figure 3A and B). Then, taking the top 5 most abundant flora as the dominant flora in each group, Circos plots were used to show the correspondence between samples and flora, the dominant flora composition in each group, and the distribution of each dominant flora among different groups. At the phylum level, the abundances of *p_Firmicutes and p_Actinobacteriota* were higher in both the CG and XG than in MG, while *p_Bacteroidota* and *p_Proteobacteria* were fewer in the CG and XG than in the MG. At the genus level, the abundance of *g_Lactobacillus* was higher in both CG and XG than that in MG, whereas the abundance of *g_Muribaculaceae_unclassified* was lower in both CG and XG than that in MG (Figure 3C and D). While these variations were observed, they were not statistically significant.

Analysis of the changes in flora among the three groups, based on the Kruskal–Wallis non-parametric test, revealed that, at the phylum level, *p_unclassified* was the only taxon showing significant inter-group variation ($P<0.01$). And at the genus level, *g_Lactobacillus* showed the highest relative abundance and significant changes across the three groups ($P<0.05$) (Figure 3E). Further Wilcoxon test analysis revealed that the relative abundance of this genus was significantly lower in the MG compared to CG ($P < 0.05$), and was higher in the XG than in the MG, although the difference was not statistically significant ($P>0.05$). In addition, compared to the CG, the MG exhibited an increase in the relative abundance of *p_Desulfobacterota* and *g_Klebsiella* ($P<0.05$). Compared to the MG, XG showed a significant decrease in the relative abundances of *p_Proteobacteria* and *g_Desulfovibrio*, whereas the relative abundances of *s_Phascolarctobacterium_faecium* and *s_Roseburia_sp*. increased ($P<0.05$) (Figure 3E). Sankey diagrams were used to visualize the relationship between and the proportion of related flora at the phylum and genus levels for each group of samples, with the width of the branches indicating the magnitude of the flux (Figure 3F).

XQJRG Corrected Intestinal Metabolic Disorders in Young Febrile Rats

PCA and OPLS-DA

A total of 25,245 peaks were extracted from all the samples, resulting in 17,442 peaks after deviation value filtering, missing value filtering and imputation, and data standardization. The differences in metabolic profiles among samples were preliminarily

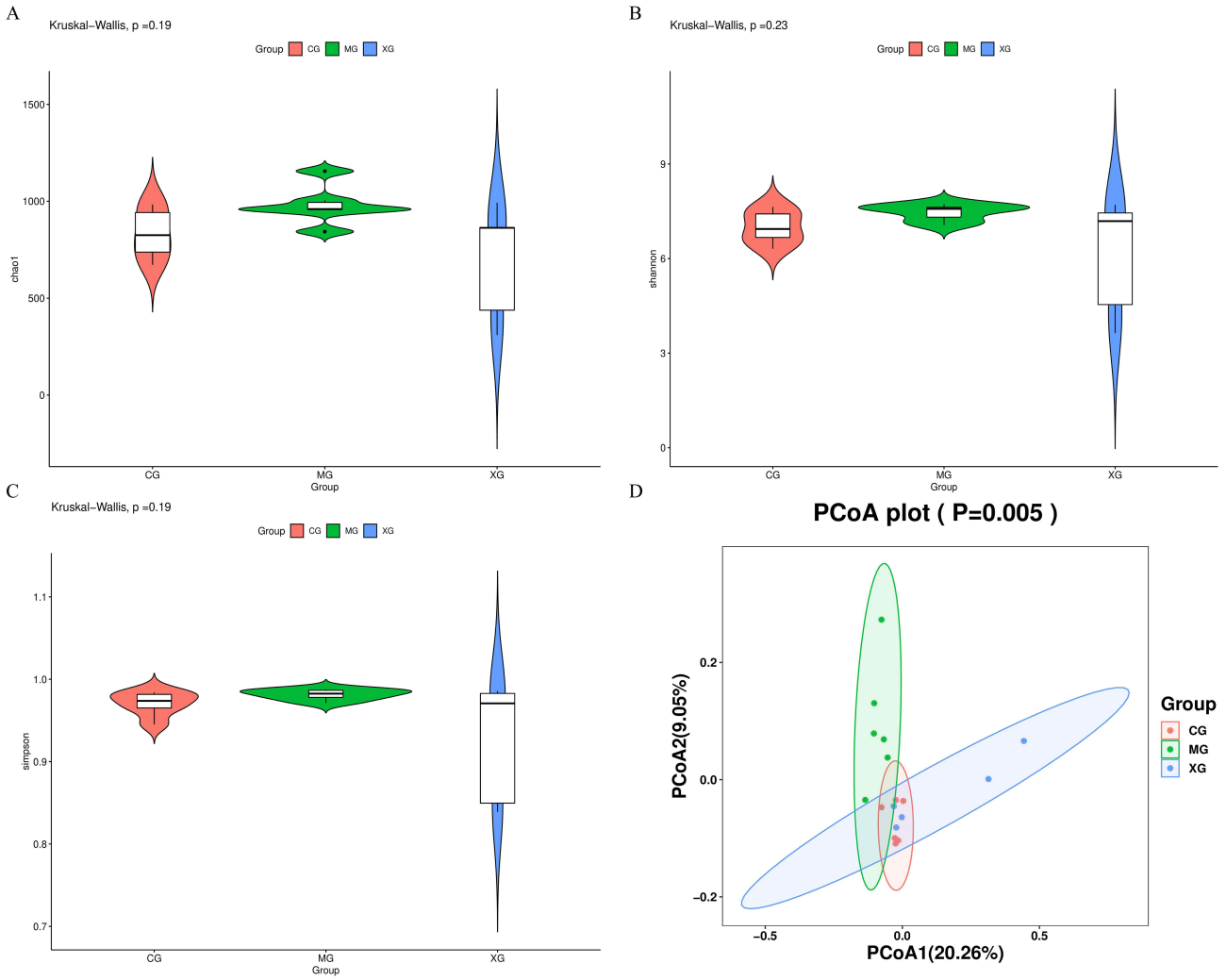

Figure 2 Diversity and variability analysis of intestinal flora in febrile young rats. (**A**) Chao1 index. (**B**) Shannon index. (**C**) Simpson index. (**D**) Principal coordinate analysis based on unweighted UniFrac distance.

assessed using PCA, revealing that all samples fell within the 95% confidence interval (Figure 4A and B). Subsequently, OPLS-DA was employed to identify genuine intergroup variances and select effective differential metabolites. OPLS-DA modeling analysis was conducted on the first principal component, with 7-fold cross-validation. The results demonstrated that the samples from MG were markedly distant from those of CG or XG horizontally, yet closely aligned vertically (Figure 4C and D), indicating substantial disparities in the intestinal metabolic profiles between MG and CG or XG. Concurrently, 7-fold cross-validation results showed R^2Y values (interpretability of the model to the categorical variable Y) of 0.985 and Q^2 values (predictability of the model) of 0.768 for the MG and CG models. The R^2Y value for the XG and MG models was 0.969 with a Q^2 value of 0.778. The R^2Y values of the two models were close to 1, implying that they could effectively elucidate the differences between the two groups. Permutation tests were conducted to validate the effectiveness of these models. As illustrated in Figure 4C, with decreasing permutation retention rates, both R^2Y and Q^2 values declined while the regression line exhibited an upward trend, suggesting the absence of overfitting in the two original models (Figure 4E and F).

Identification of Differential Metabolites

Combining univariate and multivariate analyses, differential metabolites between groups were selected based on variable importance in the projection (VIP) scores exceeding 1 in the first principal component of the OPLS-DA model, Student's *t*-test yielding *P*-values <0.05, and fold change criteria >1.5 or <0.8. The outcomes were visually represented using volcano plots (Figure 5A and B). The quantitative values of these differential metabolites were used to compute

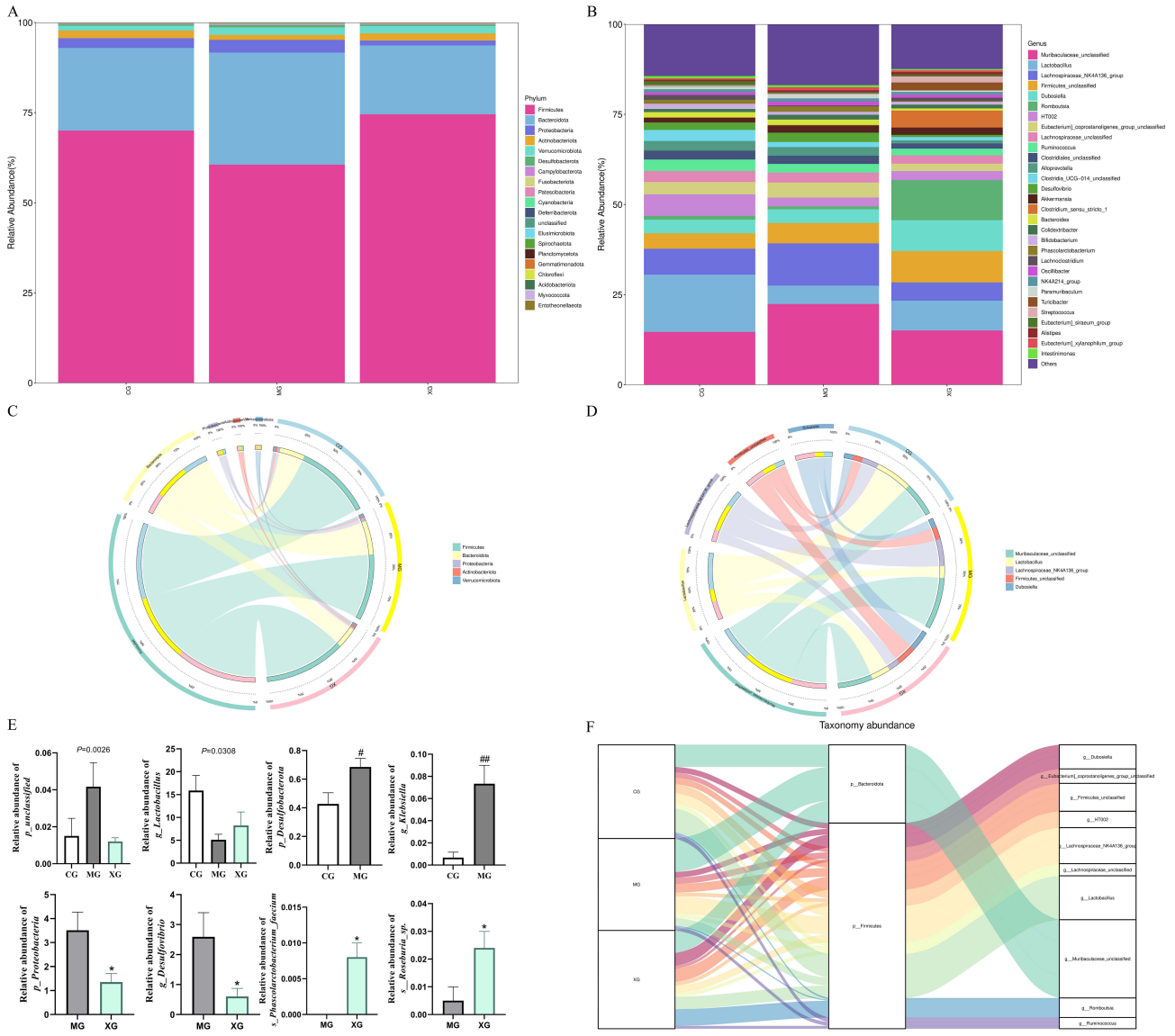

Figure 3 Composition and differential analysis of intestinal flora in young febrile rats. (**A**) The top 30 most abundant phyla in each group. (**B**) The top 30 most abundant genera in each group. (**C**) The top 5 most abundant phyla in each group. (**D**) The top 5 most abundant genera in each group. (**E**) Relative abundance of differentiated flora for comparison among groups. $^{\#}P<0.05$, $^{\#\#}P<0.01$, compared with CG; $^{*}P<0.05$, compared with MG. (**F**) Sankey diagrams of the relationship and proportion of related flora in each group at the phylum and genus levels.

a Euclidean distance matrix for clustering, as shown in the heatmap (Figure 5C and D). The quantitative values of the differential metabolites were ratio-transformed using a logarithm with a base of 2, and the top 10 alterations (including upregulation and downregulation) were depicted using a bar graph (Figure 5E and F). Furthermore, some differential metabolites with opposite trends were identified in the comparisons between MG vs CG and XG vs MG (Table 1).

Pathway Analysis

The Kyoto Encyclopedia of Genes and Genomes (KEGG) pathway database (http://www.kegg.jp/kegg/pathway.html) was used to annotate the differential metabolites and conduct metabolic pathway analyses. Based on the annotation results of the differential metabolites, the Rich Factor was calculated to analyze the degree of enrichment of the KEGG pathways, where a higher value indicated greater enrichment (Figure 6A and B). Simultaneously, to understand the overall alterations in all the differential metabolites within a pathway, the differential abundance (DA) score was computed. In the DA score plot, the lengths of the line segments represented the absolute value of the DA score. The

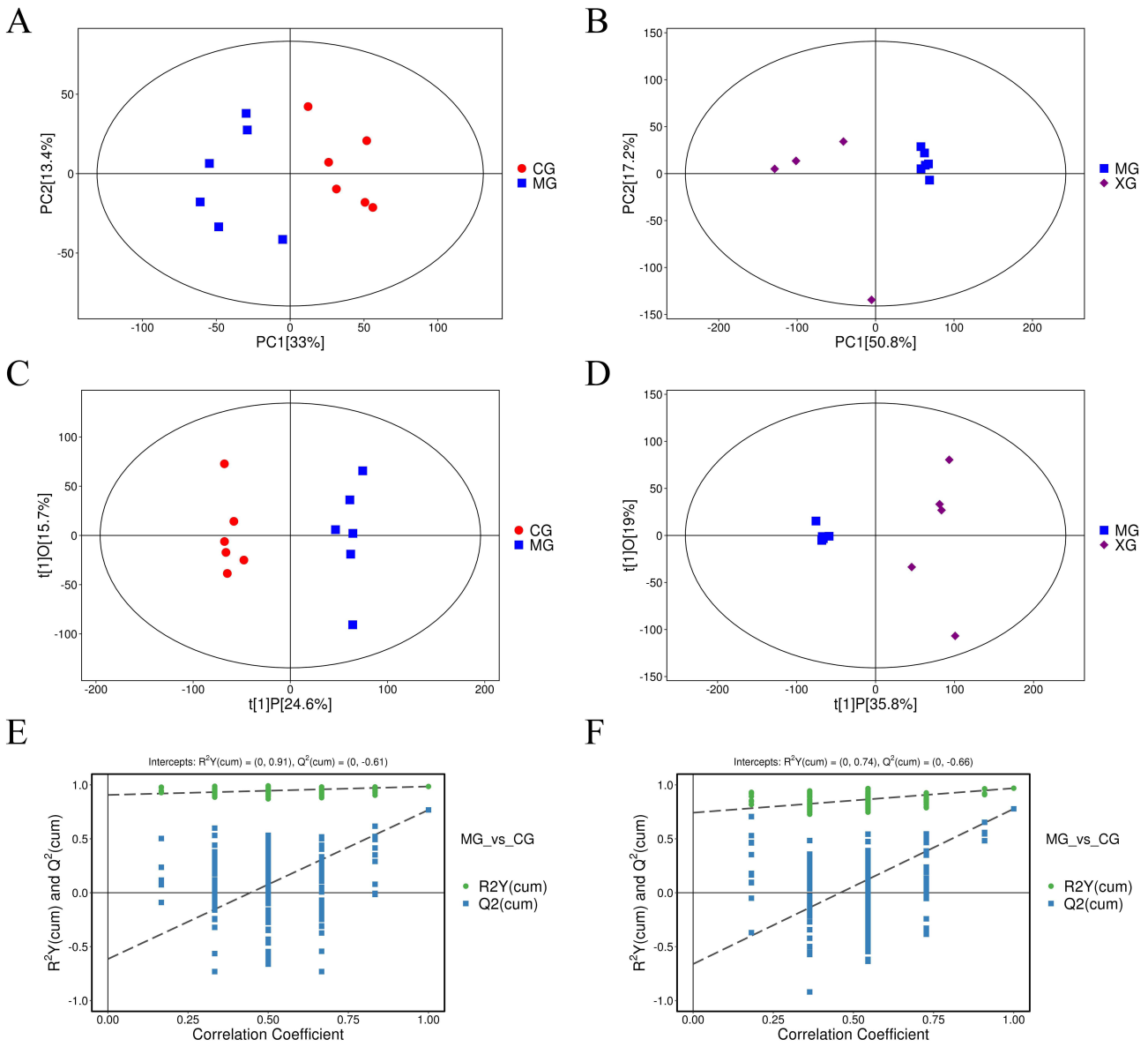

Figure 4 Scatter plots of PCA scores, scatter plots of OPLS-DA scores, and permutation test results for intestinal content samples from young febrile rats. (**A**) Score scatter plot of PCA model for MG vs CG. (**B**) Score scatter plot of PCA model for XG vs MG. (**C**) Score scatter plot of OPLS-DA model for MG vs CG. (**D**) Score scatter plot of OPLS-DA model for XG vs MG. (**E**) Permutation plot test of OPLS-DA model for MG vs CG. (**F**) Permutation plot test of OPLS-DA model for XG vs MG.

sizes of the dots indicated the number of differentially annotated metabolites in the pathway. Dots distributed to the right of the axis with longer line segments showed a tendency towards upregulation of the overall expression of the pathway; conversely, dots distributed to the left of the axis with longer line segments showed a tendency towards downregulation. As depicted in Figure 6C and D, the metabolic pathways in febrile rats were predominantly upregulated, whereas those in rats treated with XQJRG were mainly downregulated. Notably, pathways such as ATP-binding cassette (ABC) transporters, steroid hormone biosynthesis, and nucleotide metabolism were upregulated in febrile rats ($P<0.001$), but showed varying degrees of significant downregulation after XQJRG treatment. Subsequently, by mapping differential metabolites to authoritative metabolite databases, such as KEGG, the Human Metabolome Database (HMDB), and PubChem, a comprehensive analysis, including enrichment and topological analyses of the pathways in which the differential metabolites reside, was conducted. This analysis revealed that histidine metabolism and steroid hormone biosynthesis were the key pathway most strongly associated with the differential metabolite profiles in MG vs CG and XG vs MG, respectively (Figure 6E and F).

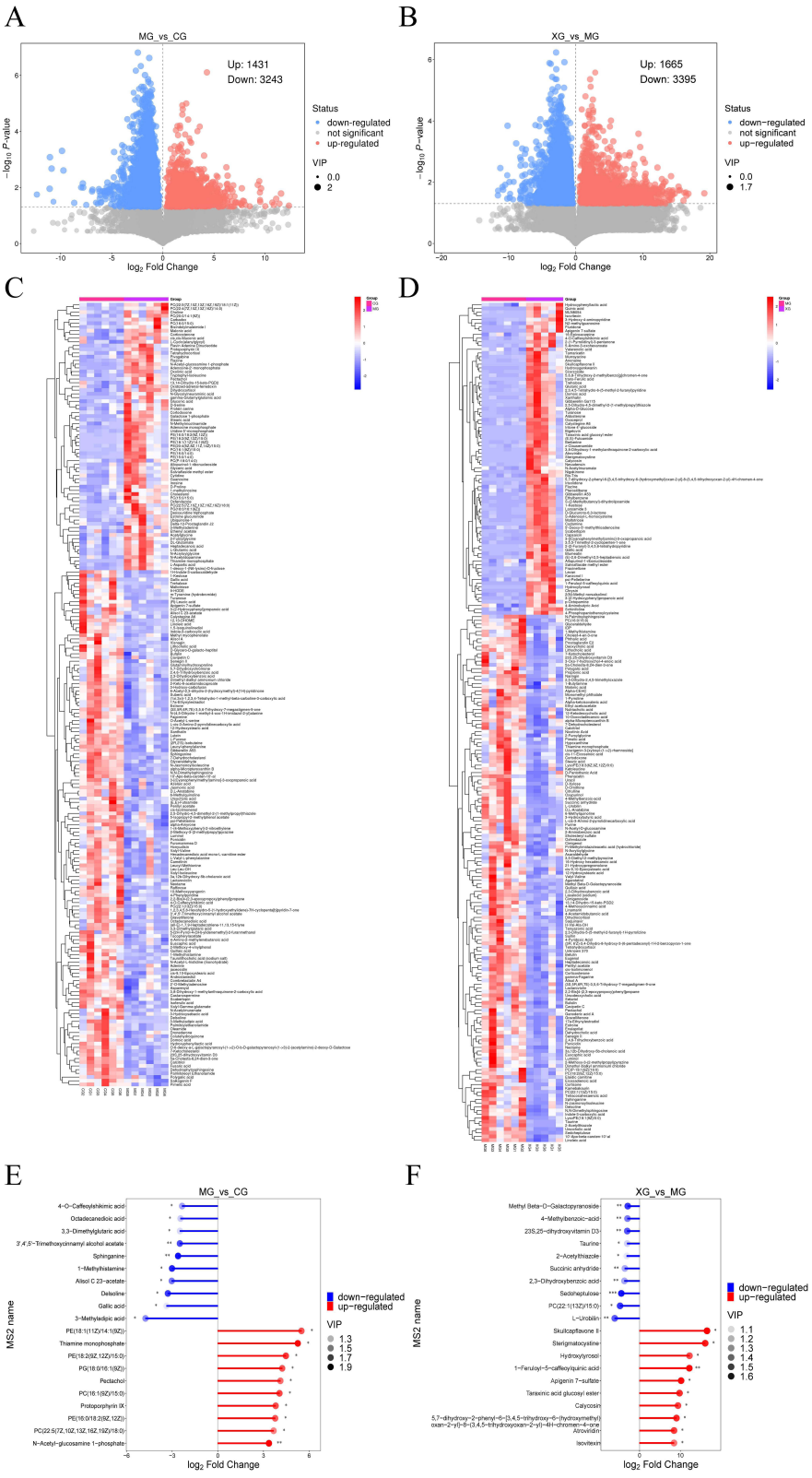

Figure 5 Differential metabolites in the intestinal metabolic profile of young febrile rats. (**A**) Volcano plot of differential metabolites of MG vs CG. (**B**) Volcano plot of differential metabolites of XG vs MG. (**C**) Clustering heat map of differential metabolites of MG vs CG. (**D**) Clustering heat map of differential metabolites of XG vs MG. (**E**) Top 10 differential metabolites of change in MG vs CG. (**F**) Top 10 differential metabolites of change in XG vs MG. *0.01<*P*<0.05, ** 0.001<*P*<0.01, *** *P*<0.001.

Table 1 Effects of XQJRG on Intestinal Metabolites in Young Febrile Rats

NO.	Differential metabolites	m/z	Rt (s)	VIP	Trend in MG [a]	Trend in XG [b]
1	Gallic acid	169.01	20.69	1.12	↓	↑
2	4-O-Caffeoylshikimic acid	337.09	196.43	1.35	↓	↑
3	Apigenin 7-sulfate	351.02	17.03	1.22	↓	↑
4	Domoic acid	312.14	128.42	1.62	↓	↑
5	Trehalose	360.15	235.22	1.66	↓	↑
6	Turanose	341.11	262.92	1.66	↓	↑
7	(E,E)-Futoamide	302.17	162.34	1.41	↓	↑
8	3-(2-Hydroxyphenyl)propanoic acid	165.06	39.15	1.36	↓	↑
9	Gibberellin A53	347.19	155.44	1.75	↓	↑
10	Calystegine A6	160.10	164.48	1.58	↓	↑
11	N-Acetylmuramate	292.10	213.75	1.31	↓	↑
12	Psi-Pelletierine	154.12	39.86	1.46	↓	↑
13	Hydroxyphenyllactic acid	181.05	109.37	1.78	↓	↑
14	Xanthatin	229.12	262.68	1.36	↓	↑
15	3-[(Cyanophenylmethyl)amino]-3-oxopropanoic acid	219.08	133.46	1.44	↓	↑
16	3,8-Dihydroxy-1-methylanthraquinone-2-carboxylic acid	299.05	22.09	1.53	↓	↑
17	Scabertopin	376.17	115.22	1.58	↓	↑
18	Maltotriose	503.16	264.73	1.43	↓	↑
19	1-Kestose	503.16	248.62	1.28	↓	↑
20	2,5-Dihydro-4,5-dimethyl-2-(1-methylpropyl)thiazole	172.12	172.23	1.15	↓	↑
21	Heptadecanoic acid	269.25	23.38	1.37	↑	↓
22	13,14-Dihydro-15-keto-PGD2	351.22	128.39	1.37	↑	↓
23	Malonic acid	103.00	233.48	1.60	↑	↓
24	Tetrahydrocortisol	425.25	38.43	1.37	↑	↓
25	2-Furoylglycine	168.03	234.14	1.54	↑	↓
26	N-Acryloylglycine	130.05	249.39	1.65	↑	↓
27	Cortodoxone	347.22	86.75	1.41	↑	↓
28	Corticosterone	347.22	105.96	1.71	↑	↓
29	Oxfendazole	314.06	105.83	1.66	↑	↓
30	Dihydrocortisol	363.22	105.30	1.60	↑	↓
31	Stearic acid	283.26	22.83	1.80	↑	↓
32	PC(16:0/15:0)	720.55	45.50	1.58	↑	↓
33	Pectachol	443.23	49.06	1.54	↑	↓
34	Thiamine monophosphate	345.08	284.14	1.87	↑	↓

Note. "↓" indicates decreased, and "↑" indicates increased; a, compared with the CG; b, compared with the MG.

Potential Biomarker Identification

Receiver operating characteristic (ROC) curves were used to evaluate and screen potential biomarkers. Typically, the closer the area under the ROC curve (AUC) value is to 1, the higher the predictive accuracy, with an AUC >0.9 indicating a high diagnostic value for the metabolite. The information regarding the AUC, 95% confidence interval (95% CI), sensitivity, and specificity of differential metabolites of MG vs CG and XG vs MG were presented in Tables 2 and 3. Among these, corticosterone and dihydrocortisol were shared between the two comparative groups; both were significantly upregulated in young febrile rats and were subsequently significantly downregulated by XQJRG. Figure 7 illustrated a comparison of the relative abundance and ROC curves. This suggested that they serve not only as biomarkers for young febrile rats but also as crucial indicators for understanding the mechanism of XQJRG treatment.

XQJRG Modulated the Levels of Intestinal SCFAs in Young Febrile Rats

As crucial metabolic byproducts of the intestinal microbiota, SCFAs play a vital role in the host immune metabolic system. Therefore, we identified and quantified SCFAs using GC-MS/MS. The results revealed increases in the levels of

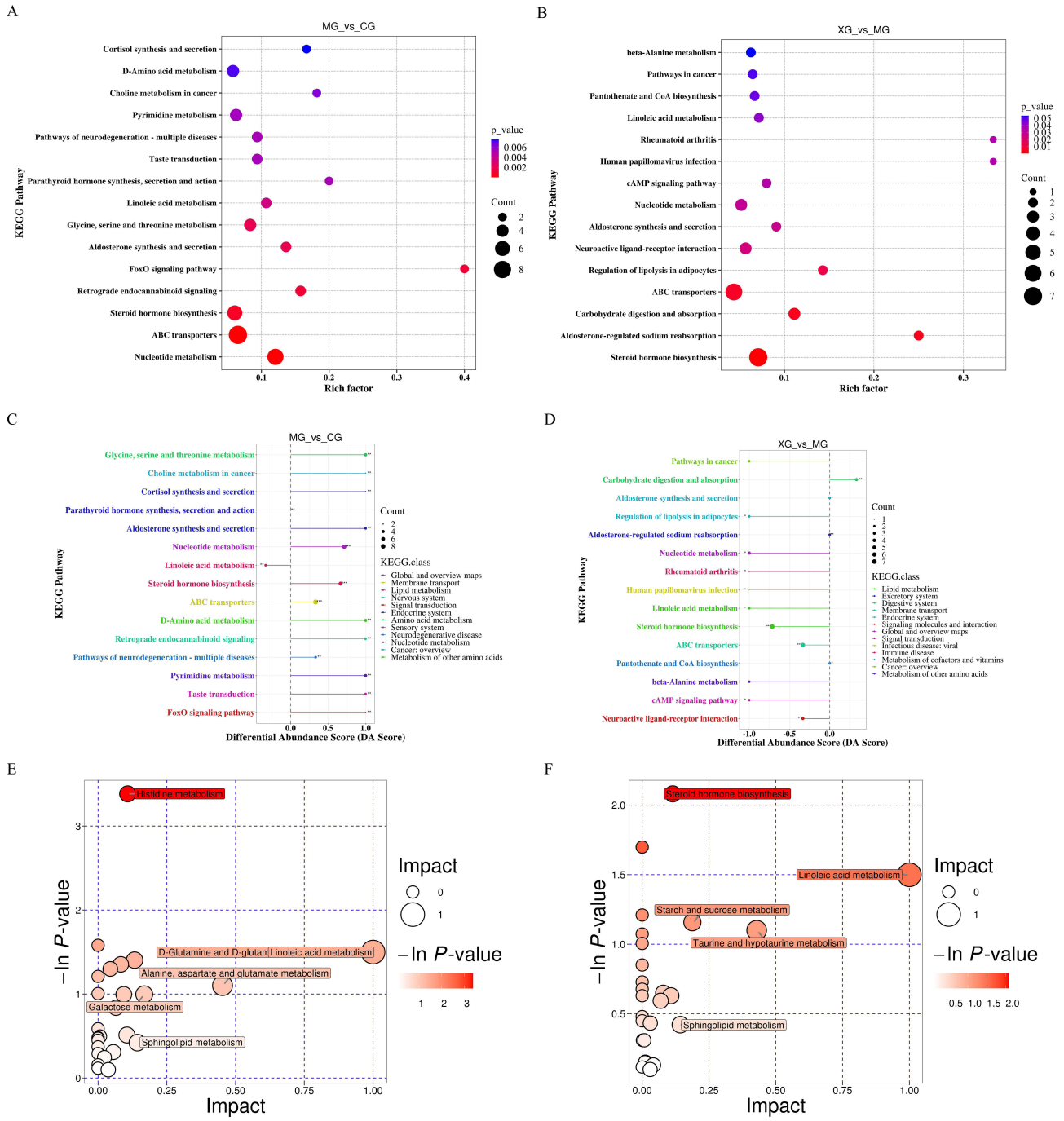

Figure 6 Analysis of KEGG metabolic pathways. (**A**) Pathway enrichment plot of differential metabolites in MG vs CG. (**B**) Pathway enrichment plot of differential metabolites in XG vs MG. (**C**) Pathway differential abundance score plot of differential metabolites in MG vs CG. ** 0.001<*P*<0.01, *** *P*<0.001. (**D**) Differential abundance score plot of differential metabolites in pathways in XG vs MG. *0.01<*P*<0.05, ** 0.001<*P*<0.01, *** *P*<0.001. (**E**) Bubble plots of pathway synthesis analysis of differential metabolites in MG vs CG. (**F**) Bubble plots of pathway synthesis analysis of differential metabolites in XG vs MG.

valeric acid and heptanoic acid in MG compared to those in CG ($P<0.05$). Valeric acid levels were decreased ($P<0.05$) and butyric acid and nonanoic acid levels were increased in XG compared to MG ($P<0.05$). Furthermore, as illustrated in Figure 8, XQJRG exhibited a tendency to pull back in changes to eight of the eleven SCFAs, although the differences were mostly statistically insignificant.

Table 2 Potential Biomarkers in Young Febrile Rats (MG Vs CG)

Name	AUC	CI(0.95)	Specificity	Sensitivity	Trend
Corticosterone	1.00	1--1	1	1	Up
Dihydrocortisol	1.00	1--1	1	1	Up
Malonic acid	1.00	1--1	1	1	Up
Tryptophyl-Isoleucine	0.97	0.90–1	1	0.83	Up
N-Acetyl-glucosamine 1-phosphate	1.00	1--1	1	1	Up
2-Furoylglycine	1.00	1--1	1	1	Up
L-Aspartic acid	1.00	1--1	1	1	Up
1-deoxy-1-(N6-lysino)-D-fructose	1.00	1--1	1	1	Up
N-Acryloylglycine	1.00	1--1	1	1	Up
Oxfendazole	0.94	0.82–1	0.83	1	Up
Leucyl-phenylalanine	1	1--1	1	1	Down
L-Fucose	1	1--1	1	1	Down
N-Jasmonoylisoleucine	1	1--1	1	1	Down
Gibberellin A53	1	1--1	1	1	Down
(2R,2'S)-Isobuteine	1	1--1	1	1	Down
N,N-Dimethylsphingosine	1	1--1	1	1	Down
Isoferulic acid	1	1--1	1	1	Down
Calcitriol	1	1--1	1	1	Down
7-Dehydrocholesterol	1	1--1	1	1	Down
Alpha-Micropteroxanthin B	1	1--1	1	1	Down

Table 3 Potential Biomarkers for XQJRG Antipyretic Therapy (XG Vs MG)

Name	AUC	CI(0.95)	Specificity	Sensitivity	Trend
Corticosterone	1	1--1	1	1	Down
Sedoheptulose	1	1--1	1	1	Down
Lithocholic acid	1	1--1	1	1	Down
10'-Apo-beta-caroten-10'-al	1	1--1	1	1	Down
Gamma-Fagarine	1	1--1	1	1	Down
Dihydrocortisol	1	1--1	1	1	Down
Ursocholic acid	1	1--1	1	1	Down
Betulin	1	1--1	1	1	Down
Tenuazonic acid	1	1--1	1	1	Down
Tetrahydrocortisol	1	1--1	1	1	Down
Schinifoline	1	1--1	1	1	Up
N2-methylguanosine	1	1--1	1	1	Up
Bis-Tris	1	1--1	1	1	Up
1-Feruloyl-5-caffeoylquinic acid	1	1--1	1	1	Up
4-Phosphopantothenoylcysteine	1	1--1	1	1	Up
2(N)-Methyl-norsalsolinol	1	1--1	1	1	Up
Hydroxyphenyllactic acid	1	1--1	1	1	Up
Alpha-D-Glucose	1	1--1	1	1	Up
Pterostilbene	0.90	0.69–1	1	0.8	Up
3-[(Cyanophenylmethyl)amino]-3-oxopropanoic acid	1	1--1	1	1	Up

XQJRG Inhibited the Intestinal Inflammatory Response in Young Febrile Rats

SCFAs such as butyric acid and nonanoic acid exhibit potent anti-inflammatory activity, and the efficacy of XQJRG in inhibiting inflammatory responses in febrile rats has been previously demonstrated. To ascertain whether XQJRG influences intestinal immunity through modulation of SCAFs, qPCR was employed to assess alterations in the

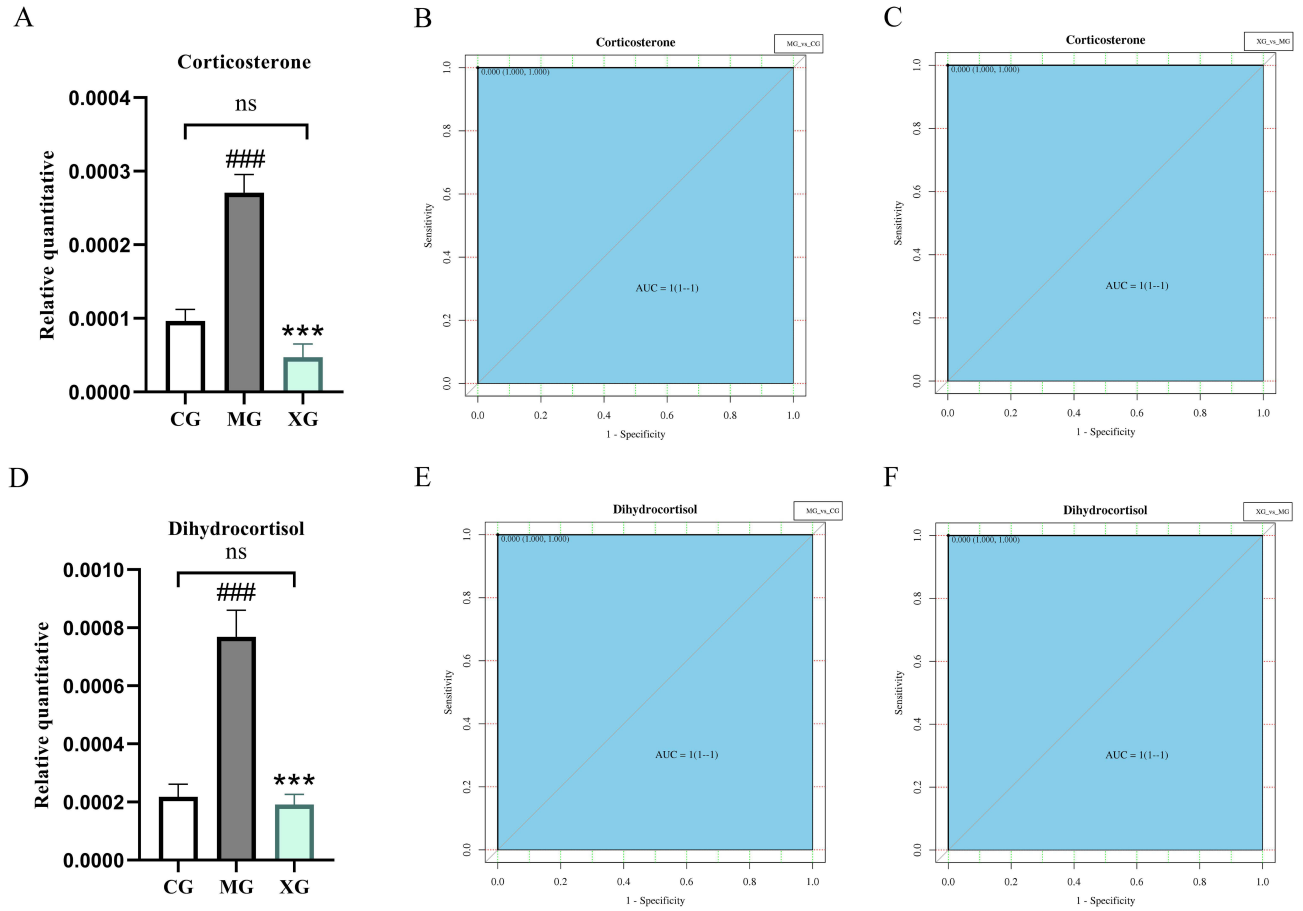

Figure 7 Histograms of the relative levels of corticosterone (**A-C**) and dihydrocortisol (**D-F**) and the corresponding ROC curves. (**A**) Histogram of the relative quantitative of corticosterone in the three groups. (**B**) ROC curve of corticosterone between MG and CG. (**C**) ROC curve of corticosterone between XG and MG. (**D**) Histogram of the relative quantitative of dihydrocortisol in the three groups. (**E**) ROC curve of dihydrocortisol between MG and CG. (**F**) ROC curve of dihydrocortisol between XG and MG. Ns, not significant between CG and XG. $^{###}P<0.001$, compared with CG; $^{***}P<0.001$, compared with MG.

transcriptional levels of SCFAs receptors GPR41, GPR43, GPR109A, and inflammatory factors IL-1β, IL-6, IL-18, and MCP-1 in the colon. As shown in Figure 9, compared to the CG, the mRNA expression levels of GPR41 in the MG were decreased ($P<0.05$), while the mRNA expression levels of IL-1β and MCP-1 were markedly increased ($P<0.001$). Following XQJRG treatment, the relative expression levels of all three genes were reduced ($P<0.001$). Subsequent analysis of WB grayscale values confirmed a decrease in GPR41 protein levels in young febrile rats ($P<0.05$), which was increased after XQJRG treatment ($P<0.05$). ELISA results confirmed an increase in the pro-inflammatory factors IL-1β ($P<0.01$) and MCP-1 ($P<0.05$) in young febrile rats, which were reduced after treatment by XQJRG ($P<0.001$, $P<0.05$, respectively).

Discussion

Previous research has indicated a sustained decline in body temperature within 6 hours of XQJRG treatment in febrile rats, accompanied by a substantial presence of flavonoid compounds in their plasma.[9] To further investigate the antipyretic efficacy of XQJRG in young febrile rats, the duration of temperature monitoring was extended in this study. The results revealed that 6–10 hours post-treatment, rats administered XQJRG continued to exhibit a decreasing trend in body temperature, approaching normal. Conversely, after an initial decline, rats in the BG showed an upward trend in body temperature, gradually resembling that of febrile rats. This finding not only aligns with clinical dosing practices, where ibuprofen typically requires dosing every 4–6 hours and TCM is administered twice daily, but also underscores the advantage of XQJRG over ibuprofen in reducing body temperature without subsequent fever rebound.

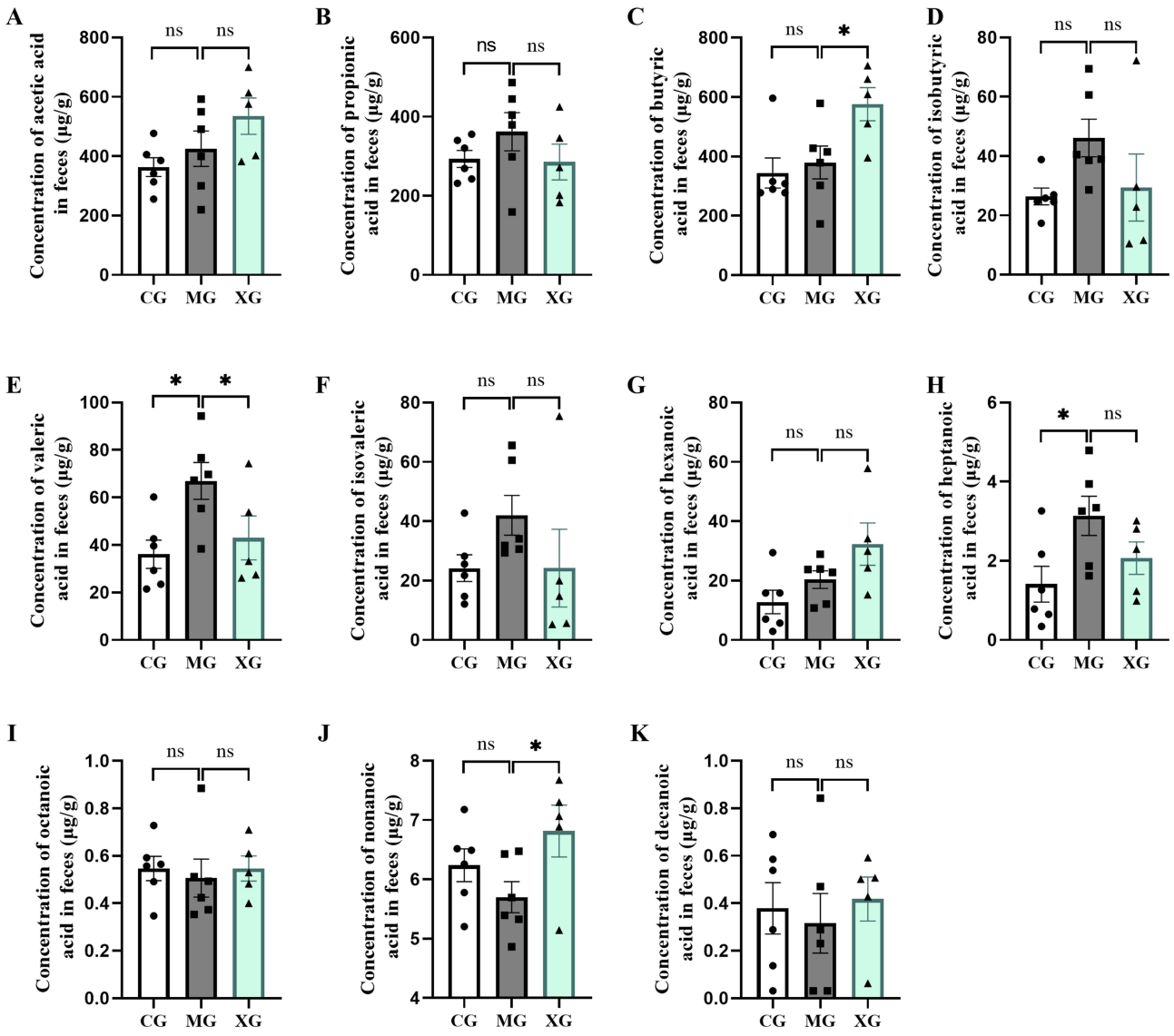

Figure 8 The absolute content of SCFAs in colonic feces of young febrile rats. (**A**) Acetic acid. (**B**) Propionic acid. (**C**) Butyric acid. (**D**) Isobutyric acid. (**E**) Valeric acid. (**F**) Isovaleric acid. (**G**) Hexanoic acid. (**H**) Heptanoic acid. (**I**) Octanoic acid. (**J**) Nonanoic acid. (**K**) Decanoic acid. Ns, not significant; *P< 0.05.

Fever has been demonstrated to affect the gut microbiota of various animals, including humans. Febrile dependency-related alterations in the gut microbiota have been observed in severe cases of COVID-19.[1] According to previous reports, compared to normal children, those with cold/fever exhibited a significant increase in the relative abundance of *Erysipelatoclostridium* and a notable decrease in *Lachnospiraceae_UCG-001* in the gut.[22] Moreover, a prospective study suggested that infants with higher microbial maturity and diversity at six months had a lower incidence of fever in the subsequent six months.[23] However, the overall interaction between childhood fever and gut microbiota remains inadequately explored. In this study, there were no statistically significant differences in α-diversity of gut microbiota among groups, indicating a limited impact of short-term fever on flora richness and diversity of gut microbiota in young rats. Nevertheless, beta-diversity analysis revealed distinct differences among febrile, normal, and XQJRG-treated rats, with the latter two groups exhibiting greater similarity. Subsequent analysis of the gut microbiota composition also showed that at both the phylum and genus levels, the dominant microbiome and relative abundance of XQJRG-treated and normal rats appeared to be more similar across the three groups. Furthermore, in the dominant flora analysis, the relative abundances of *p_Firmicutes* and *p_Actinobacteriota* decreased in febrile rats, while abundance of *p_Bacteroidota* and *p_Proteobacteria* increased. This differed slightly from previous studies that found a decrease in

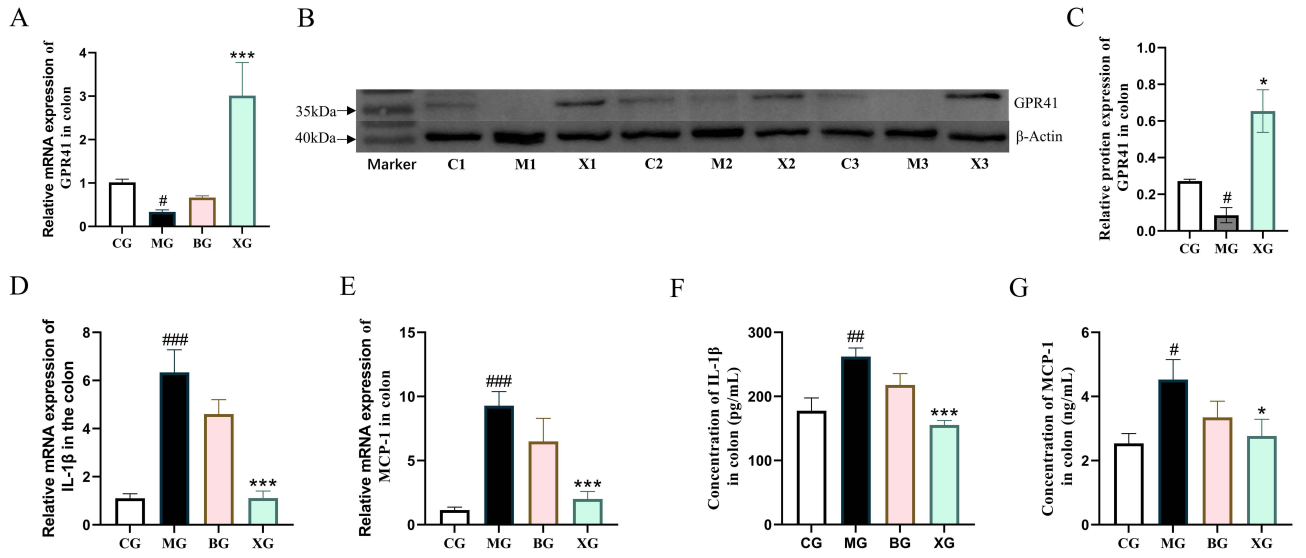

Figure 9 Levels of GPR41, IL-1β, and MCP-1 in the colon of young febrile rats. (**A**) Relative mRNA expression of GPR41. (**B**) Protein content of GPR41. (**C**) Relative protein expression levels of GPR41. (**D**) Relative mRNA expression levels of IL-1β. (**E**) Relative mRNA expression of MCP-1. (**F**) Concentration of IL-1β. (**G**) Concentration of MCP-1. Data are presented as the mean ± SEM. Compared to CG, $^{\#}P<0.05$, $^{\#\#}P<0.01$ and $^{\#\#\#}P<0.001$; Compared to MG, * P <0.05, ***P<0.001.

Bacteroidetes and an increase in *Actinobacteria* in febrile rats compared to normal rats.[20] This variation may stem from differences in the animal model selection and fever induction methods. Gao et al induced fever in adult Wistar rats via intraperitoneal injection of lipopolysaccharide (LPS) solution, whereas our study induced fever in young SD rats via subcutaneous injection of a yeast suspension. Literatures have reported a decrease in *Firmicutes* and an increase in *Proteobacteria* in various animals during heat stress.[24] Additionally, it has been reported that dysbiosis in inflammatory bowel disease manifests as decreased *Firmicutes* and increased *Proteobacteria* and *Bacteroidetes*.[25] *Firmicutes* are primary producers of anti-inflammatory SCAFs,[26] whereas *Proteobacteria* have been shown to be positively associated with gut inflammation.[27] These results indicated that young febrile rats had an imbalance in the intestinal microbiota, which could be reversed by XQJRG treatment.

Specifically, among the significantly altered microbiota in the three groups, the highest relative abundance was observed in *g_Lactobacillus*, which was reduced in young febrile rats and increased after XQJRG treatment. The probiotic bacterium *g_Lactobacillus* is widely recognized for its immunomodulatory properties. According to previous reports, infants fed *Lactobacillus reuteri* formula have fewer incidences of fever and diarrhea than those fed non-probiotic formula, thus preventing infantile infections.[28] A randomized, controlled, double-blind clinical trial of 198 children aged 2–5 years showed that children taking *Lactobacillus rhamnosus* CRL1505 had fewer fevers and a lower incidence of respiratory and intestinal infections compared to those taking placebo.[29] Furthermore, compared to normal rats, young febrile rats showed a significant increase in the conditional pathogenic bacteria *g_Klebsiella* and *g_Parasutterella* in the gut. Among the multiple taxa that were significantly reduced by XQJRG in young febrile rats, the highest relative abundance was observed in *g_Desulfovibrio*, a potentially harmful gut bacterium.Extensive research has indicated that *Desulfovibrio* is a pathogenic agent of bacteremia that affects the pathophysiology and extra-intestinal spread of various infectious diseases.[30] Interestingly, it has been reported that *Lactobacillus acidophilus* KLDS1.0901 within *g_Lactobacillus* can inhibit the abundance of *Desulfovibrio* in the gut. Moreover, XQJRG treatment significantly increased the relative abundance of *s_Phascolarctobacterium_faecium* and *s_Roseburia_sp*. They are closely related to the production of SCFAs in the intestine.[31] Especially *s_Roseburia_sp*. is a key bacterium in colonic butyric acid production.[32] Overall, gut dysbiosis occurred in young febrile rats and was characterized by changes in dominant flora, a reduction in beneficial bacteria, and an increase in opportunistic pathogens, whereas XQJRG treatment aided in restoring homeostasis.

Acute fever in children is typically caused by infection and is accompanied by activation of the immune system and inflammatory response. The gut microbiota not only participates in immunomodulation by influencing the host metabolic

system, but also mediates the metabolism of orally administered herbal medicines in vivo into metabolites with enhanced activity and immunomodulatory properties. In this study, the PCA and OPLS-DA scatter plots of the first principal component in both group comparisons (MG/CG and XG/MG) exhibited substantial separation, indicating significant changes in the intestinal metabolic profile of young febrile rats, with 139 metabolites significantly decreased and 72 metabolites significantly increased. Similarly, the intestinal metabolome of young febrile rats treated with XQJRG showed significant alterations, with 83 metabolites significantly upregulated and 143 metabolites significantly downregulated. Among these metabolites, 34 exhibited opposite trends in the changes between the comparisons of MC/CG and XG/MG, which were thought to be closely associated with the therapeutic effects of XQJRG. The metabolites significantly increased by XQJRG: gallic acid, apigenin 7-sulfate, scabertopin, 1-kestose, xanthatin, trehalose, calystegine A6, and hydroxyphenyllactic acid all possess anti-inflammatory or immunomodulatory properties. According to reports, gallic acid attenuated inflammation by reducing the release of inflammatory cytokines, chemokines, and adhesion molecules.[33] Apigenin 7-sulfate is a sulfated derivative of apigenin, a flavonoid compound renowned for its antioxidant and anti-inflammatory properties.[34] Scabertopin, a sesquiterpene lactone, exhibited superior anti-inflammatory effects compared with indomethacin in LPS-induced RAW 264.7 cells.[35] Supplementation with 1-kestose, the smallest oligofructose, significantly increased the number of intestinal lactobacilli in mice, thereby influencing both the intestinal and systemic immune responses and significantly enhancing butyrate production in rats.[36,37] Xanthatin, another sesquiterpene lactone, has been shown to inhibit the inflammatory effects in LPS-induced RAW 264.7 cells, with its mechanism linked to the downregulation of nuclear factor kappa-B signaling pathways.[38] Trehalose has been reported to significantly reduce levels of pro-inflammatory cytokines IL-1β, IL-6, and TNF-α in LPS-stimulated macrophages, inhibiting the transcriptional activity of COX-2, thereby reducing the production of inflammatory mediator PGE2.[39,40] Furthermore, levels of anti-inflammatory compounds in the gut of young febrile rats, such as skullcapflavone II, calycosin, isovitexin, capsaicin, chrysin, berberine, nevadensin, levan, fraxinellone, and fluridone, were significantly elevated after XQJRG treatment.[41–50] It is notable that capsaicin not only affected intestinal immune homeostasis, but also influenced the composition, abundance, and function of intestinal microbiota, increasing the content of *Roseburia* and *Lactobacilli*, possibly contributing to the significant increase in the relative abundance of *s_Roseburia* with XQJRG treatment.[48] Conversely, the levels of metabolites directly associated with fever, such as 13.14-Dihydro-15-keto-PGD2 and PGE2, were significantly decreased by XQJRG treatment. 13.14-Dihydro-15-keto-PGD2 is a metabolite of PGD2, and peripheral PGD2 has been shown to contribute to LPS-induced fever.[51] PGE2, as a recognized inflammatory mediator, not only upregulates the thermoregulatory set point in the hypothalamus under central induction but also promotes intestinal inflammation by inhibiting microbiota-dependent regulatory T cells.[52] These findings suggested that XQJRG likely inhibited the inflammatory response in young febrile rats by modulating the crosstalk between the intestinal microbiota and metabolites.

The association between fever and metabolic hyperactivity has been well recognized.[53] This was consistent with the predominant upregulation of metabolic pathways observed in young febrile rats in the present study. In contrast, metabolic pathways were overwhelmingly downregulated after XQJRG treatment, suggesting that XQJRG corrected the yeast-induced intestinal hypermetabolic state in young febrile rats. Among these pathways, ABC transporters, steroid hormone biosynthesis, and nucleotide metabolism exhibited significantly opposite trends in young febrile rats and those treated with XQJRG. This phenomenon was also observed by Gao et al, in which potential biomarkers involving ABC transporters and nucleotide metabolism were implicated in febrile rats compared with normal rats or those treated with antipyretic Chinese medicine.[20] ABC transporters participate in the transport of lipopolysaccharides and inflammatory lipid mediators that play crucial roles in the immune system.[54] The extracellular release of nucleotides is associated with inflammatory responses, and studies have shown that alterations in cyclic nucleotide metabolism are related to prostaglandin synthesis in rat colonic tissues.[55] Moreover, while steroid hormone biosynthesis is typically thought to occur mainly in organs, including the adrenal glands, gonads, and brain, studies have confirmed the local production of glucocorticoids (GC) in intestinal mucosal tissues in response to immune system activation, aiding in balancing immune responses and preventing tissue damage.[56] In view of the low baseline synthesis of GC in the intestines, immune stress and initiation of inflammation can strongly promote their synthesis, suggesting that locally produced GC in the intestines may represent a negative feedback loop that regulates and maintains immune homeostasis. In febrile children with body

temperature >38.3°C, a significant decrease in serum cortisol concentration was observed with recovery from infection, with an average change of up to 3.6-fold compared to the time of presentation.[57] SD and Wistar rats also exhibited an increase in plasma corticosterone levels with increasing core body temperature during fever.[58,59] Moreover, this was supported by the identification of potential biomarkers for the differential metabolites in this study. The levels of corticosterone and dihydrocortisol in the rat intestines significantly increased after fever onset and returned to normal levels after XQJRG treatment. Therefore, corticosterone and dihydrocortisol can be considered important biomarkers in young febrile rats and for the therapeutic effects of XQJRG.

Based on the aforementioned evidence suggesting that XQJRG may exert its effects by modulating the intestinal immune metabolic system, we conducted high-throughput targeted detection of SCFAs, metabolites with anti-inflammatory activity. It was found that XQJRG had regulatory effects on multiple SCFAs, significantly elevating the levels of butyric acid and nonanoic acid in young febrile rats and markedly reducing the level of valeric acid. Previous studies have indicated that butyric acid, a crucial mediator of host-microbiota crosstalk, enhances intestinal innate immune function via receptors including GPR41, GPR43, and GPR109A, while mitigating excessive inflammatory responses by inhibiting histone deacetylases.[60] In vitro experiments demonstrated that butyrate salts significantly attenuated the increase in IL-1β, IL-6, and TNF-α levels in LPS-induced RAW 264.7 cells,[61] and the expression of IL-1β, IL-6, and COX-2 in bovine macrophages.[62] Nonanoic acid has been reported to upregulate endogenous defense peptides in the intestine, thereby enhancing the immunological barrier function of epithelial cells.[63] Surprisingly, the levels of valeric acid in the colons of normal and XQJRG-treated rats were significantly lower than those in young febrile rats. Valeric acid has previously been considered a histone deacetylase inhibitor with potential anti-inflammatory properties.[64] However, the literature has also reported an increase in blood valeric acid levels in both young and aged mice following transplantation of gut microbiota from aged mice, leading to exacerbated ischemic brain injury and inflammation. And inhibiting the increase in interleukin 17 induced by valeric acid could alleviate inflammation and improve survival curves.[65] Therefore, the immunomodulatory role of valeric acid produced by intestinal microbiota may be complex and warrants further investigation.

The molecular biology experiments revealed elevated transcription and protein levels of the pro-inflammatory cytokines IL-1β and MCP-1 in the colon, indicating activation of local immune and inflammatory responses in young febrile rats. Treatment with XQJRG significantly upregulated the expression levels of the SCFA receptor GPR41 and markedly downregulated the mRNA and protein expression of IL-1β and MCP-1, suggesting that the therapeutic effect of XQJRG is at least partially associated with modulating the intestinal immune response under febrile conditions. Interestingly, XQJRG exhibited the most pronounced inhibitory effect on IL-1β in both peripheral circulation and the intestine. Clinical reports in pediatric influenza and colds have shown correlations between IL-1β levels and the severity of illness,[66] and IL-1β plays a central role in modulating disease-related behaviors in febrile animals.[67] This aspect should be explored further in future studies.

Given the limited research on the crosstalk between fever and intestinal microbiota and its metabolites in children or young animals, our study provides new insights into this area. Overall, dysbiosis of the intestinal microbiota in young febrile rats during fever manifested as a reduction in *p_Firmicutes*, an increase in *p_Bacteroidetes* and *p_Proteobacteria*, a decrease in beneficial bacteria such as *g_Lactobacillus*, and an increase in opportunistic pathogens including *g_Klebsiella* and *g_Parasutterella*. Alongside this process, most metabolic pathways were upregulated, including ABC transporters, steroid hormone biosynthesis, and nucleotide metabolism. Associated metabolites such as corticosterone and dihydrocortisol may serve as biomarkers in young febrile rats. Furthermore, fever-induced local immune activation and inflammatory responses in the intestine, leading to increased transcription and secretion of pro-inflammatory cytokines such as IL-1β and MCP-1. In this context, XQJRG demonstrated a corrective effect on intestinal dysbiosis and metabolic disruption, thereby inhibiting intestinal inflammation. However, our study had certain limitations. For example, we did not conduct fecal microbiota transplantation experiments to explore the contribution of the intestinal microbiota and its metabolites to the antipyretic and anti-inflammatory effects of XQJRG. Additionally, temperature regulation during fever involves bidirectional communication between the central and peripheral systems, and we did not elucidate the communication between the intestinal microbiota and the central nervous system following XQJRG treatment. Therefore, we consider these areas as future research directions.

Conclusion

Young rats exhibited intestinal flora dysbiosis and hypermetabolism during fever. XQJRG treatment restored the relative abundance of the dominant bacterial *p_Firmicutes*, decreased the relative abundance of inflammation-associated *p_Bacteroidetes* and *p_Proteobacteria*, and increased the abundance of the beneficial bacterium *g_Lactobacillus* that was significantly reduced in febrile rats, thus bringing their intestinal bacterial profile closer to that of normal rats. XQJRG also significantly decreased the relative abundance of the harmful intestinal bacterium *g_Desulfovibrio* and significantly increased the relative abundance of the SCFA-producing flora *s_Phascolarctobacterium_faecium* and *s_Roseburia_sp*. Meanwhile, XQJRG significantly increased the levels of metabolites with anti-inflammatory or immunomodulatory effects, including gallic acid, skullcapflavone II, and berberine, as well as the levels of butyric acid and its receptor GPR41. Consequently, the levels of metabolites directly associated with fever, such as 13.14-Dihydro-15-keto-PGD2 and PGE2, were significantly reduced, and the levels of the pro-inflammatory cytokines IL-1β and MCP-1 in the colon were normalized. In summary, XQJRG exerted antipyretic and anti-inflammatory effects in young febrile rats by modulating the gut microbiota and host metabolism.

Data Sharing Statement

The data that support the findings of this study are available on request from the corresponding author, Lei Xiong, upon reasonable request.

Acknowledgment

We would like to thank Editage (www.editage.cn) for English language editing. The graphical abstract was drawn using Figdraw (www.figdraw.com).

Author Contributions

All authors made a significant contribution to the work reported, whether that is in the conception, study design, execution, acquisition of data, analysis and interpretation, or in all these areas; took part in drafting, revising or critically reviewing the article; gave final approval of the version to be published; have agreed on the journal to which the article has been submitted; and agree to be accountable for all aspects of the work.

Funding

This work was supported by the National Natural Science Foundation of China (82374523, 82074421, and 82160924), the Key R&D Program of Yunnan Province Science and Technology Department (202103AC100005), the State Administration of Traditional Chinese Medicine's high-level key discipline construction project of traditional Chinese medicine ([2023] No. 85), Qihuang Scholars - National TCM Leading Talent Support Program ([2022] No. 6), National Famous Traditional Chinese Medicine Experts Inheritance Studio Construction Project ([2022] No. 75), 2023 Yunnan Province Postgraduate Tutor Team Building Project ([2023] No. 8), the Applied Basic Research Programs of Science and Technology Commission Foundation of Yunnan Province (202301AS070084), the Project of First-class Discipline Construction in Yunnan Province (2022YB03), and the Yunnan Provincial Academician and Expert Workstation (202105AF150037), Scientific Research Fund Project of Yunnan Provincial Department of Education (2024Y378).

Disclosure

All authors declare that they have no known competing financial interests or personal relationships that could have appeared to influence the work reported in this paper.

References

1. Zhou Y, Shi X, Fu W, et al. Gut Microbiota Dysbiosis Correlates with Abnormal Immune Response in Moderate COVID-19 Patients with Fever. *J Inflamm Res*. 2021;14:2619–2631. doi:10.2147/JIR.S311518
2. Ding K, Sun E, Huang R, et al. Integrated metabolome-microbiome analysis investigates the different regulations of Pudilan Xiaoyan oral liquid in young rats with acute pharyngitis compared to adult rats. *Phytomedicine*. 2023;120:155037. doi:10.1016/j.phymed.2023.155037

3. I ALKASSAA. *New Insights on Antiviral Probiotics: From Research to Applications*. Switzerland: Springer; 2017. doi:10.1007/978-3-319-49688-7_1
4. Bongers KS, Chanderraj R, Woods RJ, et al. The gut microbiome modulates body temperature both in sepsis and health. *Am J Respir Crit Care Med*. 2023;207(8):1030–1041. doi:10.1164/rccm.202201-0161OC
5. Kong X, Wan H, Su X, et al. Rheum palmatum L. and Coptis chinensis Franch, exert antipyretic effect on yeast-induced pyrexia rats involving regulation of TRPV1 and TRPM8 expression. *J Ethnopharmacol*. 2014;153(1):160–168. doi:10.1016/j.jep.2014.02.007
6. Ma L, Liu H, Luo C, et al. Fever and antipyretic supported by traditional Chinese medicine: a multi-pathway regulation. *Front Pharmacol*. 2021;12:583279. doi:10.3389/fphar.2021.583279
7. Wang D, Shi M, Hu H, et al. Clinical research report on traditional Chinese patent medicines and traditional Chinese classic famous prescriptions (2022). *Acupuncture and Herbal Medicine*. 2024;4(3):306–319. doi:10.1097/HM9.0000000000000122
8. Huang S, Luo C, Xu R, et al. *Study on the Antipyretic Activity and Potential Mechanism of Indigo Naturalis on Lipopolysaccharide-Induced Fever Rat Model*; 2023. doi:10.21203/rs.3.rs-3174972/v1
9. He X, Cui J, Li H, et al. Antipyretic effects of Xiangqin Jiere granules on febrile young rats revealed by combining pharmacodynamics, metabolomics, network pharmacology, molecular biology experiments and molecular docking strategies. *J Biomol Struct Dyn*. 2024;1–18. doi:10.1080/07391102.2024.2301761
10. Nie J, Hu W, Li G,Ke J, and, Xiong L. Antipyretic Effect of Xiangqin Jiere Granules on Yeast-Induced Febris Rats. *China J Tradition Chin Med Pharm*. 2017;32(10):4692–4695.
11. Nie J, Li G, Zhang J, Hu W, Xiong L. Antipyretic Effect of Xiangqin Jiere Granule on 2,4-Dinitrophenol Induced Febris Rats. *Chinese J Tradit Med Scie Techn*. 2018;25(4):477–480.
12. Nie J, Ke J, Zhang J, Liang L, Hu W, Xiong L. Positive and Negative Regulation on Body Temperature of Xiangqin Jiere Granules on Pyretic Rabbits Induced by Endotoxin. *China J Tradition Chin Med Pharm*. 2019;34(1):304–307.
13. Wang Y. Clinical study on the treatment of infantile common cold fever with Xiangqin Antipyretic Granule [master's thesis]. Kunming: Yunnan University of Chinese Medicine; 2019. Chinese.
14. Zhou X, Li G, Xiong L, Nie J. Study on the Clinical Efficacy of Xiangqin Jiere Granules in the Treatment of Pediatric Cold and Fever. *J Yunnan Universit Tradi Chi Medi*. 2016;39(2):61–65. doi:10.19288/j.cnki.issn.1000-2723.2016.02.017
15. Lu Y, Xie J, Peng C, Wang B, Wang K, Li L. Enhancing Clinical Efficacy through the Gut Microbiota: a New Field of Traditional Chinese Medicine. *Engineering*. 2019;5(1):40–49. doi:10.1016/j.eng.2018.11.013
16. Jung MA, Jang SE, Hong SW, Hana MJ, Kim DH. The role of intestinal microflora in anti-inflammatory effect of baicalin in mice. *Biomol Ther*. 2012;20(1):36–42. doi:10.4062/biomolther.2012.20.1.036
17. Gao T, Zhang H, Li Q, et al. Fuzi decoction treats chronic heart failure by regulating the gut microbiota, increasing the short-chain fatty acid levels and improving metabolic disorders. *J Pharm Biomed Anal*. 2023;236:115693. doi:10.1016/j.jpba.2023.115693
18. Liu H, Feng C, Yang T, et al. Combined metabolomics and gut microbiome to investigate the effects and mechanisms of Yuquan Pill on type 2 diabetes in rats. *J Chromatogr B Analyt Technol Biomed Life Sci*. 2023;1222:123713. doi:10.1016/j.jchromb.2023.123713
19. Liu J, Wang X, Li Q, et al. Fecal metabolomics combined with 16S rRNA gene sequencing to analyze the effect of Jiaotai pill intervention in type 2 diabetes mellitus rats. *Front Nutr*. 2023;10:1135343. doi:10.3389/fnut.2023.1135343
20. Gao Y, Liu L, Li C, et al. Study on the Antipyretic and Anti-inflammatory Mechanism of Shuanghuanglian Oral Liquid Based on Gut Microbiota-Host Metabolism. *Front Pharmacol*. 2022;13:843877. doi:10.3389/fphar.2022.843877
21. Yang Y, Lu W, Zhang X, Wu C. Gut fungi differentially response to the antipyretic (heat-clearing) and diaphoretic (exterior-releasing) traditional Chinese medicines in Coptis chinensis-conditioned gut microbiota. *Front Pharmacol*. 2022;13:1032919. doi:10.3389/fphar.2022.1032919
22. Liu CE, Pan YM, Du ZL, et al. Composition characteristics of the gut microbiota in infants and young children of under 6 years old between Beijing and Japan. *Transl Pediatr*. 2021;10(4):790–806. doi:10.21037/tp-20-376
23. Kortekangas E, Young R, Cheung YB, et al. A Prospective Study on Child Morbidity and Gut Microbiota in Rural Malawi. *J Pediatr Gastroenterol Nutr*. 2019;69(4):431–437. doi:10.1097/MPG.0000000000002435
24. Huus KE, Ley RE, Gilbert JA. Blowing Hot and Cold: body Temperature and the Microbiome. *mSystems*. 2021;6(5):e0070721. doi:10.1128/mSystems.00707-21
25. Davenport M, Poles J, Leung JM, et al. Metabolic Alterations to the Mucosal Microbiota in Inflammatory Bowel Disease. *Inflamm Bowel Dis*. 2014;20(4):723–731. doi:10.1097/MIB.0000000000000011
26. Feng W, Ao H, Gut Microbiota PC. Short-Chain Fatty Acids, and Herbal Medicines. *Front Pharmacol*. 2018;9:1354. doi:10.3389/fphar.2018.01354
27. Rizzatti G, Lopetuso LR, Gibiino G, Binda C, Gasbarrini A, Canducci F. Proteobacteria: a Common Factor in Human Diseases. *Biomed Res Int*. 2017;9351507. doi:10.1155/2017/9351507
28. Weizman Z, Asli G, Alsheikh A. Effect of a probiotic infant formula on infections in child care centers: comparison of two probiotic agents. *Pediatrics*. 2005;115(1):5–9. doi:10.1542/peds.2004-1815
29. Villena JC, Salva MS, Nuñez MS, et al. Probiotics for everyone! The novel immunobiotic Lactobacillus rhamnosus CRL1505 and the beginning of Social Probiotic Programs in Argentina. *Int J Biotechnol Wellness Ind*. 2012;189–198. doi:10.6000/1927-3037/2012.01.03.05
30. Singh SB, Carroll-Portillo A, Lin HC. *Desulfovibrio* in the Gut: the Enemy within? *Microorganisms*. 2023;11(7):1772. doi:10.3390/microorganisms11071772
31. Wu F, Guo X, Zhang J, Zhang M, Ou Z, Peng Y. Phascolarctobacterium faecium abundant colonization in human gastrointestinal tract. *Exp Ther Med*. 2017;14(4):3122–3126. doi:10.3892/etm.2017.4878
32. Duncan SH, Barcenilla A, Stewart CS, Pryde SE, Flint HJ. Acetate utilization and butyryl coenzyme A (CoA): acetate-CoA transferase in butyrate-producing bacteria from the human large intestine. *Appl Environ Microbiol*. 2002;68(10):5186–5190. doi:10.1128/AEM.68.10.5186-5190.2002
33. Bai J, Zhang Y, Tang C, et al. Gallic acid: pharmacological activities and molecular mechanisms involved in inflammation-related diseases. *Biomed Pharmacother*. 2021;133:110985. doi:10.1016/j.biopha.2020.110985
34. Ginwala R, Bhavsar R, Chigbu DGI, Jain P, Khan ZK. Potential Role of Flavonoids in Treating Chronic Inflammatory Diseases with a Special Focus on the Anti-Inflammatory Activity of Apigenin. *Antioxidants*. 2019;8(2):35. doi:10.3390/antiox8020035

35. Wu Z, Zhang Y, Chen N, et al. Sesquiterpene lactones from Elephantopus mollis and their anti-inflammatory activities. *Phytochemistry*. 2017;137:81–86. doi:10.1016/j.phytochem.2017.01.020
36. Tochio T, Kadota Y, Tanaka T, Koga Y. 1-Kestose, the Smallest Fructooligosaccharide Component, Which Efficiently Stimulates Faecalibacterium prausnitzii as Well as Bifidobacteria in Humans. *Foods*. 2018;7(9):140. doi:10.3390/foods7090140
37. Yoshida N, Satou W, Hata S, et al. Effects of 1-Kestose and Nystose on the Intestinal Microorganisms and Immune System in Mice. *J Appl Gerontol*. 2006;53(3):175–180. doi:10.5458/jag.53.175
38. Liu Y, Chen W, Zheng F, Yu H, Wei K. Xanthatin Alleviates LPS-Induced Inflammatory Response in RAW264.7 Macrophages by Inhibiting NF-κB, MAPK and STATs Activation. *Molecules*. 2022;27(14):4603. doi:10.3390/molecules27144603
39. Taya K, Hirose K, Hamada S. Trehalose inhibits inflammatory cytokine production by protecting IκB-α reduction in mouse peritoneal macrophages. *Arch Oral Biol*. 2009;54(8):749–756. doi:10.1016/j.archoralbio.2009.05.003
40. Yu S, Park H, Kim W. Trehalose Inhibits Inflammatory Responses through Mitochondrial Reprogramming in RAW 264.7 Macrophages. *Antioxidants*. 2023;12(6):1166. doi:10.3390/antiox12061166
41. Brahmachari GN. Isolation, chemistry and bioactivity. *Int J Green Pharm*. 2010;4(4):213. doi:10.22377/ijgp.v4i4.150
42. Gong G, Zheng Y, Yang Y, Sui Y, Wen Z, Cioanca O. Pharmaceutical Values of Calycosin: one Type of Flavonoid Isolated from *Astragalus*. *Evid Based Complement Alternat Med*. 2021;9952578. doi:10.1155/2021/9952578
43. Kim J, Park Y, Shin J, et al. Fraxinellone inhibits lipopolysaccharide-induced inducible nitric oxide synthase and cyclooxygenase-2 expression by negatively regulating nuclear factor-kappa B in RAW 264.7 macrophages cells. *Biol Pharm Bull*. 2009;32(6):1062–1068. doi:10.1248/bpb.32.1062
44. Kumar A, Mukherjee M, Pottabathini R, Dhull DK, Pottabathini R, Dhull DK. Current knowledge and pharmacological profile of berberine: an update. *Eur J Pharmacol*. 2015;761:288–297. doi:10.1016/j.ejphar.2015.05.068
45. Lin C, Huang S, Liang Y, et al. Isovitexin Suppresses Lipopolysaccharide-Mediated Inducible Nitric Oxide Synthase through Inhibition of NF-kappa B in Mouse Macrophages. *Planta Med*. 2005;71(8):748–753. doi:10.1055/s-2005-871287
46. Magnone M, Scarfì S, Sturla L, et al. Fluridone as a new anti-inflammatory drug. *Eur J Pharmacol*. 2013;720(1):7–15. doi:10.1016/j.ejphar.2013.10.058
47. Naz S, Imran M, Rauf A, et al. Chrysin: pharmacological and therapeutic properties. *Life Sci*. 2019;235:116797. doi:10.1016/j.lfs.2019.116797
48. Rosca AE, Iesanu MI, Zahiu CD, Voiculescu SE, Paslaru AC, Zagrean A. Capsaicin and Gut Microbiota in Health and Disease. *Molecules*. 2020;25(23):5681. doi:10.3390/molecules25235681
49. Srikanth R, Siddartha G, Reddy CHSS S, Harish BS, Janaki Ramaiah M, Uppuluri KB. Antioxidant and anti-inflammatory levan produced from Acetobacter xylinum NCIM2526 and its statistical optimization. *Carbohydr Polym*. 2015;123:8–16. doi:10.1016/j.carbpol.2014.12.079
50. Zhao D, Ji J, Li S, Wu A. Skullcapflavone II protects neuronal damage in cerebral ischemic rats via inhibiting NF-κB and promoting angiogenesis. *Microvasc Res*. 2022;141:104318. doi:10.1016/j.mvr.2022.104318
51. Gao W, Schmidtko A, Wobst I, Lu R, Angioni C, Geisslinger G. Prostaglandin D2 produced by hematopoietic prostaglandin D synthase contributes to LPS-induced fever. *J Physiol Pharmacol*. 2009;60(2):145–150.
52. Crittenden S, Goepp M, Pollock J, et al. Prostaglandin E2 promotes intestinal inflammation via inhibiting microbiota-dependent regulatory T cells. *Sci Adv*. 2021;7(7):eabd7954. doi:10.1126/sciadv.abd7954
53. Belon L, Skidmore P, Mehra R, Walter E. Effect of a fever in viral infections - The 'Goldilocks' phenomenon? *World J Clin Cases*. 2021;9(2):296–307. doi:10.12998/wjcc.v9.i2.296
54. Kotlyarov S, Kotlyarova A. Clinical Significance of Lipid Transport Function of ABC Transporters in the Innate Immune System. *Membranes*. 2022;12(11):1083. doi:10.3390/membranes12111083
55. Craven PA, DeRubertis FR. Stimulation of rat colonic mucosal prostaglandin synthesis by calcium and carbamylcholine: relationship to alterations in cyclic nucleotide metabolism. *Prostaglandins*. 1981;21(1):65–81. doi:10.1016/0090-6980(81)90197-0
56. Kostadinova F, Schwaderer J, Sebeo V, Brunner T. Why does the gut synthesize glucocorticoids? *Ann Med*. 2014;46(7):490–497. doi:10.3109/07853890.2014.932920
57. NICKELS DA, MOORE DC. Serum Cortisol responses in febrile children. *Pediatr Infect Dis J*. 1989;8(1):16–20. doi:10.1097/00006454-198901000-00005
58. Cabrera R, Mechiel Korte S, EGWM L, et al. The amount of free corticosterone is increased during lipopolysaccharide-induced fever. *Life Sci*. 2000;66(7):553–562. doi:10.1016/s0024-3205(99)00628-1
59. Goehler LE, Gaykema RP, Hansen MK, Kleiner JL, Maier SF, Watkins LR. Staphylococcal enterotoxin B induces fever, brain c-Fos expression, and serum corticosterone in rats. *Am J Physiol Regul Integr Comp Physiol*. 2001;280(5):R1434–R1439. doi:10.1152/ajpregu.2001.280.5.R1434
60. Zhang M, Wang Y, Zhao X, Liu C, Wang B, Zhou J. Mechanistic basis and preliminary practice of butyric acid and butyrate sodium to mitigate gut inflammatory diseases: a comprehensive review. *Nutr Res*. 2021;95:1–18. doi:10.1016/j.nutres.2021.08.007
61. Wang F, Liu J, Weng T, et al. The inflammation induced by lipopolysaccharide can be mitigated by short-chain fatty acid, butyrate, through upregulation of IL-10 in septic shock. *Scand J Immunol*. 2017;85(4):258–263. doi:10.1111/sji.12515
62. Jiang L, Wang J, Liu Z, et al. Sodium butyrate alleviates lipopolysaccharide-induced inflammatory responses by down-regulation of NF-κB, NLRP3 signaling pathway, and activating histone acetylation in bovine macrophages. *Front Vet Sci*. 2020;7:579674. doi:10.3389/fvets.2020.579674
63. Wang J, Huang N, Xiong J, Wei H, Jiang S, Peng J. Caprylic acid and nonanoic acid upregulate endogenous host defense peptides to enhance intestinal epithelial immunological barrier function via histone deacetylase inhibition. *Int Immunopharmacol*. 2018;65:303–311. doi:10.1016/j.intimp.2018.10.022
64. Yuille S, Reichardt N, Panda S, Dunbar H, Mulder IE, Nie D. Human gut bacteria as potent class I histone deacetylase inhibitors in vitro through production of butyric acid and valeric acid. *PLoS One*. 2018;13(7):e0201073. doi:10.1371/journal.pone.0201073
65. Zeng X, Li J, Shan W, Lai Z, Zuo Z. Gut microbiota of old mice worsens neurological outcome after brain ischemia via increased valeric acid and IL-17 in the blood. *Microbiome*. 2023;11(1):204. doi:10.1186/s40168-023-01648-1
66. Chiaretti A, Pulitanò S, Barone G, et al. IL-1 β and IL-6 upregulation in children with H1N1 influenza virus infection. *Mediators Inflamm*. 2013;2013:495848. doi:10.1155/2013/495848
67. Harden LM, du Plessis I, Roth J, Loram LC, Poole S, Laburn HP. Differences in the relative involvement of peripherally released interleukin (IL)-6, brain IL-1β and prostanoids in mediating lipopolysaccharide-induced fever and sickness behavior. *Psychoneuroendocrinology*. 2011;36(5):608–622. doi:10.1016/j.psyneuen.2010.09.003